Universidade de Aveiro
2016

Departamento de Engenharia de Materiais e Cerâmica

Raquel Nadine Cadete Vieira

Nanopartículas de magnetite revestidas com quitosana para hipertermia magnética

Coating of magnetite nanoparticles with chitosan for magnetic hyperthermia

Universidade de Aveiro
2016

Departamento de Engenharia de Materiais e Cerâmica

Raquel Nadine Cadete Vieira

Nanopartículas de magnetite revestidas com quitosana para hipertermia magnética

Coating of magnetite nanoparticles with chitosan for magnetic hyperthermia

Tese apresentada à Universidade de Aveiro para cumprimento dos requisitos necessários à obtenção do grau de Mestre em Materiais e Dispositivos Biomédicos, realizada sob a orientação científica da Doutora Paula Celeste da Silva Ferreira, Investigadora Principal do Centro de Investigação em Materiais Cerâmicos e Compósitos da Universidade de Aveiro e do Doutor Manuel António Martins da Silva, Bolseiro de pós-Doutoramento do Centro de Investigação em Materiais Cerâmicos e Compósitos da Universidade de Aveiro

Trabalho realizado com o apoio financeiro do projeto CICECO-Instituto de Materiais de Aveiro, POCI-01-0145-FEDER-007679 (FCT UID/CTM/50011/2013), financiado por fundos nacionais através da FCT/MEC e quando aplicável cofinanciado pelo FEDER, no âmbito do Acordo de Parceria PT2020.

o júri

Presidente	Professor Doutor Manuel Almeida Valente Professor Associado da Universidade de Aveiro
Vogal - Arguente principal	Doutor Ricardo João Borges Pinto Bolseiro de Pós-Doutoramento da Universidade de Aveiro
Vogal - Orientadora	Doutora Paula Celeste da Silva Ferreira Equiparada a Investigadora Principal da Universidade de Aveiro

Acknowledgements

I would like to thank my supervisor Dr. Paula Ferreira for all the support during this work, especially in the last days.

To my supervisor, Dr. Manuel Silva, I thank for the introduction to the materials world and the initial support.

I would like to thank Prof. Liliana Ferreira and Prof. Maria de Deus Carvalho from the *Faculty of Science of the University of* Lisbon for the magnetic and hyperthermia measurements.

I would like to thank Dr. Rosário Soares from the *Laboratório Central de Análises* of University of Aveiro for her support in XRD analyses and to technical services from Department of Materials and Ceramics Engineering, namely Ana Ribeiro, Artur Sarabando and Marta Ferro.

Thank you, Celeste Azevedo for all support during the analysis of FTIR and TGA.

To my laboratory colleagues thank you, especially you Ana.

And most important, I want to thank my family, specially my Mum and Dad for all the support.

palavras-chave

Nanopartículas magnéticas, óxido de ferro, hipertermia, dopamina, quitosana, genipina, ácido cafeico.

resumo

O cancro é uma das doenças com maior ocorrência na população mundial e com uma elevada taxa de mortalidade. Os principais problemas na luta contra o cancro prendem-se com a dificuldade de diagnóstico precoce, a citotoxicidade associada aos fármacos anticancerígenos usados em quimioterapia convencional e a falta de tratamentos mais eficazes. Com o advento da nanotecnologia, tem havido um crescente interesse na aplicação de nanopartículas e nanoestruturas, nas mais diversas áreas da ciência, nomeadamente em aplicações biomédicas. Neste contexto em particular, as nanopartículas magnéticas apresentam propriedades interessantes, por exemplo, em sistemas de libertação controlada de fármaco e em hipertermia. A sua aplicação em áreas relacionadas com a saúde, como o tratamento de cancro por hipertermia magnética, passa necessariamente por uma boa caracterização das suas propriedades e pela correta avaliação das suas capacidades de libertação de energia sob a forma de calor por indução magnética.

Nesse sentido, este trabalho teve como objetivo a síntese de nanopartículas de magnetite devido a sua compatibilidade com o organismo humano e propriedades magnéticas. No entanto, devido ao seu elevado grau de agregação assim como facilidade de oxidação em meios aquosos existe uma necessidade de revestir estas partículas. Para tal, foi utilizado um biopolímero: a quitosana.

A ligação do revestimento da quitosana ao núcleo do óxido de ferro foi realizada através de dois tipos de ancoragem: através da dopamina, conhecida pela sua grande afinidade aos grupos aminas e através do ácido cafeico, por apresentar uma similaridade estrutural à dopamina.

Para a caracterização estrutural e morfológica das partículas recorreu-se à difração de raios-X (DRX), à espetroscopia de infravermelhos com transformada de Fourier (FTIR), à dispersão dinâmica da luz (DLS), ao Potencial Zeta e à microscopia eletrónica de transmissão (TEM). As propriedades magnéticas foram medidas por magnetometria de SQUID (Superconducting Quantum Interferance Device). Por fim foi avaliada a capacidade das partículas sintetizadas para aplicação em hipertermia magnética.

keywords Magnetic nanoparticles, iron oxide, hyperthermia, dopamine, chitosan, genipin, caffeic acid

abstract

Cancer is a disease with high incidence in the world population and equally with a high mortality rate. The main problems in the fight against cancer are linked to the difficulty of early diagnosis, the cytotoxicity associated with anticancer drugs used in conventional chemotherapy and the lack of more effective treatments. With the advent of nanotechnology, there has been increasing interest in the application of nanoparticles and nanostructures, in several areas of science, such as biomedicine. In this context, the magnetic nanoparticles have interesting properties in controlled drug release systems and hyperthermia. Its application in areas related to health, such as the treatment of cancer by magnetic hyperthermia, necessarily requires a good characterization of their properties and the correct assessment of their ability to release energy in the form of heat by magnetic induction.

Therefore, this study aimed the synthesis of nanoparticles of magnetite due to their biocompatibility and magnetic properties. However, due to their high degree of aggregation as well as facile oxidation in aqueous media there is a need to coat these particles. For this purpose, a biopolymer was used: chitosan. The binding of the coat to the core of the iron oxide was accomplishment through two types of anchorages molecules: dopamine, knowing for their great affinity with amine groups and through caffeic acid due to structural similarity to dopamine.

The structural and morphological characterization was performed using X-ray diffraction (DRX), Fourier transformed infrared spectroscopy (FTIR), dynamic light scattering (DLS), Zeta Potential; thermalgravimetric analysis and transmission electron microscopy (TEM). The magnetic properties were studied using a Superconducting Quantum Interference Device (SQUID) magnetometer. Finally, we evaluated the ability of some of the synthesized NPs for use in magnetic hyperthermia.

TABLE OF CONTENTS

INDEX OF FIGURES

INDEX OF TABLES

ABBREVIATIONS

AMF	Alternating Magnetic Field
AC	Alternating Magnetic Current
CAN	Ceric Ammonium Nitrate
DLS	Dynamic Light Scattering
DMSA	Dimercaptosuccinic acid
EDAC	1-Ethyl-3-(3-dimethylaminopropyl)carbodiimide
FTIR	Fourier Transform Infrared Spectroscopy
f	Frequency
FC	Field cooling
H	Magnetic Field
Hc	Coercive Field
HEMAGl	(2-{[(D-glucosamin-2-N-yl)carbonyl]oxy}ethyl methacrylate
HT	Hyperthermia
IgG	Immunoglobulin
ILP	Intrinsic Loss Power
IS	Immune System
JCPDS	Joint Committee on Powder Diffraction Standards
M	Magnetization
MES	2-(*N*-morpholino)ethanesulfonic acid
MHT	Magnetic Hyperthermia
MNPs	Magnetic Nanoparticles
Mr	Residual Magnetization
Ms	Saturation Magnetization
NPs	Nanoparticles
PNIPA	Poly(N-isopropylacrylamide)
ROS	Reactive Oxygen Species
SAR	Specific Absorption Rate
SPL	Specific Loss Power
SPM	Superparamagnetic
SQUID	Superconducting Quantum Interference Device

TEM	Transmission electron microscopy
US FDA	United States of Food and Drug Administration
VEGF	Vascular endothelial growth factor
WHO	World Health Organization
XRD	X-ray Diffraction
ZFC	Zero field cooling

INTRODUCTION

Introduction

1.1Context

In spite of all progress made in medicine, cancer remains as one of the largest global problem, representing the main cause of illness and mortality worldwide.[1] World Cancer Report 2014 predicted an increase of cancer events from 14, in 2012, to 22 millions within the next two decades.[2] Only in 2012 more than 8 millions people died as consequence of a cancer.[1] Moreover, in the report "Assessing national capacity for the prevention and control of noncommunicable diseases: global survey" concerning the period 2010–2015, the 160 countries with available data saw an increase from 47 to 63% in number of cases of cancer incidence.[3] According to World Health Organization (WHO), the most frequent types of cancers causing deaths are lung, liver, stomach, colorectal, breast and oesophageal.[1]

Such overwhelming scenario, not only have impact in the huge number of human life losses, but also in the financial costs associated to treatments and palliative cares. According to a 2015 report published in Forbes magazine, the global cancer drug market reached the US $100 billion mark in that year, and it is predicted to achieve to US $147 billion by 2018.[4]

These appalling numbers reveal the huge need for further research exploring better, safer, and more effective therapeutic and diagnostic strategies than the used so far, enhancing patient's life quality as well as extending their lifetime. The last decades were characterized by development of novel and advanced strategies to fight cancer illness. The conventional strategies commonly employed include surgery, chemotherapy, radiotherapy, stem cell transplant therapy, immunotherapy, and other varieties of targeted therapies.[4] Despite the considerable progress in the developing cancer therapeutics, their harmful side effects are of dominant concern. Osteoporosis, infertility, premature ovarian failure, typhlitis, hair loss, herpesviridae infections, heart diseases, gastrointestinal lesions, gastric pain are few examples of possible side effects of the current therapies.[4] One of the most worrying side effects is the resistance that tumour can acquire from the recurrent use of chemotherapeutic agents in therapies.[5,6]

In an attempt to improve human's health, nanotechnology applied to medicine has been proposed in the last decades.[7] Nanomedicine, allows to work at molecular and cellular levels,

having the potential to achieve important developments in healthcare.[8] The nanomaterials have been in the few years a remarkable role in cancer diagnostic and therapeutic, where the magnetic nanoparticles (MNPs) have been in the spotlight due to their unique properties.[7–9] MNPs easily match with biomolecules and can be manipulated, for example, by an external magnetic gradient,[10] being used for magnetic resonance imaging as contrast agents,[11–15] or they can be applied as drug delivery carriers[14,16–18] for localized chemotherapy, for bioseparation,[19–21] tissue repairing[22] and thermal tumour therapy.[23–26]

1.2 Literature Review

1.2.1. Cancer

Cancer is characterized by abnormal cell growth[9] where many environment and genetic-related factors are involved.[7] When tumour cells first appear, their regular supply of oxygen and nutrients is provided by the normal blood supply of the host organ, in which the tumour ascends. As the tumour expands, it is developed its own functional vascular supply by angiogenesis.[27] However, the vasculature that is formed is primitive, chaotic and with a numerous structural and functional abnormalities.[27,28] The tumour cells are not able to fulfil their increasing demand for oxygen and nutrients.[9,28–30]. As a consequence of the hypoxic medium[31], the tumour cells tends to be more acidotic,[9,27] a feature that make the cells more susceptible to thermal damage.[31]

The development of the tumour cells mostly happens in localized tissue, but can spread to distant sites within the body by a metastatic growth. In this case, the tumour is referred as "malignant" and is usually associated with a poor prognosis for the patient,[7,9]

Although the tumour cells are more vulnerable to temperature, the hostile microenvironment where the tumour cells developed make them to exhibit resistance to therapies as radiation or even certain types of chemotherapies.[27,31]

1.2.2. Nanotechnology

Nanotechnology is the understanding and control of matter at nanometric dimensions.[10,32,33] When reducing all three dimensions of a particle of a certain composition to the nanoscale, zero dimensional nanoparticles (NPs)[34] and obtained and the original properties are usually modified. As a consequence of the dimensionality (1-100 nm),[7,13,35] they are characterized by high surface area,[7,35] which potentiates the interaction with surrounding molecules[31] and size in the range of biomolecule entities. NPs can be very attractive for biomedical applications.[35] They may be specifically targeted toward cancer cells, offering a major advantage over other therapeutic agents.[7]

The behaviours in nanoscale are not necessarily predicted from those observed in macroscopic scale. News phenomena may be observed,[10,35,36] because properties such as melting point, fluorescence, electrical conductivity, magnetic permeability, and chemical reactivity change as a function of the size. More, the nanoscale materials have larger surface areas than similar masses of larger-scale materials, which allows a greater amount of the material that can interact with surrounding materials, thus affecting reactivity.[37]

1.2.3. Magnetic materials

Magnetic materials can be classified in one of five types of magnetism: ferromagnetic, diamagnetic, paramagnetic, antiferromagnetic and ferrimagnetic[38,39] (Figure 1.1). The type of magnetism is dependent on the magnetic moments response to the application of an external applied magnetic field.[38] Ferromagnetic materials display electron spins aligned parallel to each other at absolute zero. When the Curie temperature (Tc) is reached, the ferromagnetism disappears and the material turns paramagnetic. Under cooling, the ferromagnetic domains reform and the materials become ferromagnetic again. An antiferromagnetic behaviour corresponds to the antiparallel alignment of equal moments. If the antiparallel moments have different magnitudes, the materials are called ferrimagnetic.

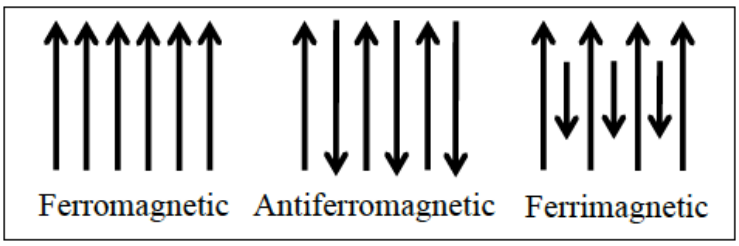

Figure 1.1 Scheme of the dipole alignment in zero applied field at room temperature for: (a) ferromagnetic, antiferromagnetic and ferrimagnetic materials.

1.2.3.1 The M-H curve

The magnetization (M) and demagnetization of a material under the applied magnetic field (H) is represented as a curve designed the *M-H* curve.[40–43] The characteristic shape of a *M-H* curve is sigmoidal and depends of the temperature and the magnetic field[41]. For high

values of *H*, the magnetization (*M*) approach to the saturation value (*Ms*) and will not increase no matter how strong *H* could be,[41,44] because in that condition- the saturation, all domains are aligned.[45] But not all the magnetic domains return to their original orientation when the applied magnetic field is reduced after reaching the Ms. Thus, when *H* returns to zero, there is a residual magnetization named remanent magnetization (*Mr*) which can be removed by applying a reverse magnetic field, called coercive field, *Hc*.[43,45] So, open hysteresis represents an irreversible process of magnetization which is related with both intrinsic (e.g., particle size, shape, and magnetocrystalline anisotropy) and structural characteristics (e.g., grain boundaries, impurities, and vacancies) of the magnetic material.[43,44] Typically, big particles (at micrometer range) lead to large hysteresis loops, while small particles lead to narrow hysteresis loops.[41] A single magnetization/demagnetization cycle (a→b→c) produces a thermal energy proportional to the shaded area within the hysteresis loop[46] (Figure 1.2).

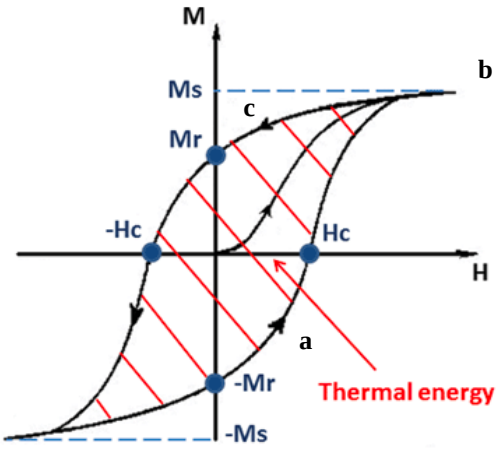

Figure 1.2 Typical hysteresis loop observed during magnetization/demagnetization of magnetic nanoparticles. M and H are magnetic flux density and magnetic field strength, respectively. A single magnetization/demagnetization cycle (a→b→c) produces a thermal energy proportional to the shaded area within the hysteresis loop.[46]

1.2.3.2 Magnetism at nanoscale

In bulk materials, the magnetic moments are divided in multiple domains (Figure 1.3a). As the particle size decreases, the domains sizes also reduce. Below a certain particle size value (denoted as critical size), the magnetic moments become organized in mono-domains

(Figure 1.3a). These mono-domains haves a more favourable energetic configuration,[6] displaying different magnetic behaviours according to temperature. Below the blocking temperature, the superparamagnetic (SPM) NPs behave as a ferromagnetic, showing a typical hysteresis loop with net magnetization (black line in Figure 1.3b). For temperatures above the blocking temperature, the remanent magnetization becomes equal to zero as well as the coercive field (blue line in Figure 2.3b).[10,13,46] The characteristic *M-H* curve of SPM NPs at room temperature is an overlap curve of curves with sigmoidal curve. When a magnetic field is applied to the SPM NPs, the magnetic moments tend to be oriented in the direction of the field, which from a certain value, leads all magnetic moments to be aligned parallel to their direction, reaching *Ms*. As the field is reduced, there is no *Mr*, and therefore no hysteresis loop[47,48] as show in Figure 1.3b.

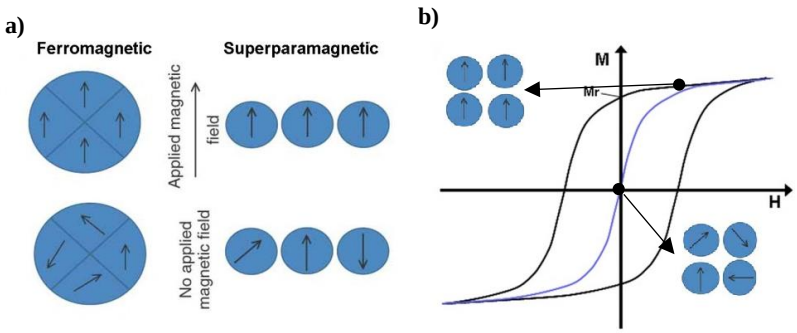

Figure 1.3 a) Multidomains and monodomains representation under application and absence of a magnetic field. (b) Magnetization curves as function of the magnetic field for superparamagnetic particles under temperatures below de blocking temperature – ferromagnetic behaviour (black line) showing hysteresis loop; and above the blocking temperature - superparamagnetic behaviour (blue line) with no remanent magnetization (M_r) and no coercive field (H_C).

The conversion of AMF energy to heat through SPM NPs are explained essentially by two theories: Néel relaxation and Brownian relaxation[9,31] (Figure 1.4). The first one causes energy to be released when the magnetic dipole of a particle flips between two stable orientations within a magnetic field that are separated by an energy barrier.[31,46,49] This physical hindrance is directly proportional to size of the particles.[49] The Brownian losses is due to random collision with other particles and the medium (like extracellular or complex components inside the cells that tends to counter the physical rotation of the suspended MNPs) and physical rotation of particles within an AMF.[5,9,10,31,46] In a SPM NPs the Brownian fluctuations are sufficiently intense to randomly orient the individual magnetic

moments of each particle, leading to a zero global magnetization.[50] The Brownian loss is not directly related to the magnetism of the SPM MNPs, but can increasingly modulate it as the particle diameter increases within the SPM range.[5]

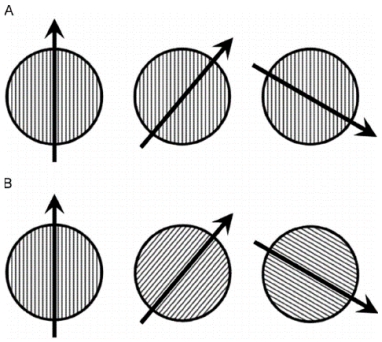

Figure **1.4** Néel rotation vs. Brownian rotation. (A) Néel rotation: the magnetic moment (arrow) rotates while the particle remains fixed (inner circle). (B) Brownian rotation: the magnetic moment (arrow) remains fixed with respect to the crystalline axes (lines inside the circle) while the particle rotates.[51]

1.2.4. Hyperthermia

The concept that heat can be used for therapeutic purposes has been described in the medical literature for centuries.[31] The increase of the temperature above normal physiological temperature (ca. 37 ºC in humans) to a mild temperature, which does not cause cell death by itself, may have therapeutic effects and be defined as hyperthermia.[28,31,52] Hyperthermia (HT) usually applies temperatures in the range of 41 to 50 ºC to induce apoptosis. Above 50 ºC is considered thermoablation.[52] Thermoablation leads to the necrosis of cancer cells, but may also affect healthy cells and therefore it is not desirable.

The success of this approach is based on the differences between healthy cells and cancer cells,[29] namely in the difference how the healthy and cancer cells behave when the temperature is increased.[52] Cells in the mitosis are sensitive to heat probably because of the injury to the mitotic apparatus.[28,52] As cancer cells have a faster cell division to quickly multiply,[10,53] making them more sensitive to the increase of temperature. The physiological differences between normal and tumour tissue in the architecture of the vasculature (quite disorganized compared to the normal tissue)[28,52,54] and with a low vessel density result in high susceptibility to the heat. In normal body temperature, the cancer cells take advantage comparatively to normal cell as the blood flow in them is faster. When the temperature

increase, the opposite happens: the blood flow in normal tissue increases whereas in the cancer tissue decreased. This happens because the cancer tissue cannot dissipate effectively the heat, remaining heated for longer time than the normal tissue. This, make the cancer cells to undergo into apoptosis phenomena, whereas normal tissue manages the high temperatures easily due to the increased blood flow.[28] All these aspects make cancer cells more susceptible to heat.[28,31] However, the specific mechanism of cell killing by hyperthermia is still unclear.[28]

The duration, homogeneity of the temperature in tissue, tissue type and context of treatment influence the effects of HT in tumour cells.[31,55] Depending on the thermal stimulation, there is a growing amount of experimental evidence showing that 43°C is the breaking point to develop cancer cell death.[32,53]

A variety of techniques have been employed to achieve HT in the modern clinic practice including electromagnetic radiation, laser, microwave, radiofrequency and high-intensity focused ultrasound.[31,43,56]

Depending on the extent of the body's exposure to heat, there are three types of HT: whole body, regional and local[5,31,42] HT. Whole body HT is achieved using water blankets and thermal chambers, whereas regional HT includes the perfusion of a tumour-bearing limb with part of the patient's blood which is taken out and warmed *ex vivo*.[5,31] Note, that these methods are not specifics and are technically challenging to perform repeatedly with reproducible heating levels. The last type of HT, the local HT, is more specific,[31] and refers to heating only one body area, usually where the tumour is located.[55,56]

1.2.4.1 Advantages and disadvantages of hyperthermia

HT is independent of the cell cycle and this is a great advantage comparing to chemotherapies, which is cytotoxic to the cells, especially in specific phases of the cell cycle. Furthermore, HT can be used to treat cancer cells localized in many places like brain, thyroid, lungs, breast, prostate, hepatocellular carcinoma among others.[53,56] Also, HT activates immunological responses to tumours for eradication by the host immune response.[31]

Many clinical trials have documented that mild temperature HT can be safely administered to patients showing clinical benefits in terms of improved local control, palliation of symptoms and even overall survival. However, it is underutilized for a variety of reasons as the invasive methods of generating HT, the difficulty in maintaining temperatures at desires

levels, the lack of monitoring and modelling of HT. For example, in local HT, more specifically, luminal and interstitial HT, employ customized probes and applicators placed close to the tumour individually; it can apply a grid to achieve relatively uniform heating of the tumour; or metal antennas that are activated by an external energy source. However the placement of external heating sources usually invasive, challenging to the deep-seated tumour, and sometimes results in a nonuniform heat distribution.[31] The external heating techniques such ultrasound and electromagnetic phase arrays are not invasive like the luminal and interstitial implants but the reproducibility and uniformity heating levels are challenging.[3]

HT treatment is seen a great promise for cancer therapy, however the methods of reaching, maintaining, monitoring and modelling heating are still requiring a huge improvement.[3]

1.2.5. Magnetic Hyperthermia

Magnetic Hyperthermia (MHT) consists in applying an AMF in a magnetic fluid to produce heating through transformation of magnetic energy in thermal energy, raising the temperature in near the cancer cells.[12,15,57–60] Magnetic fluids are class of magnetic materials constituted of colloidal suspension of MNPs.[42,61] The first application of ferrofluids for hyperthermia treatment was investigated in the work of Chan *et al*.[59] in 1993.

The MNPs can be used in a specific areas of a human body by a simple direct injection to target tissue[14,42] or by tumour specific antibody targeting[42], followed by exposing to an external magnetic field.[12,36,57,62]

As mentioned before, in the location of the malignant tumour, the proliferating cells require extra supplying oxygen and nutrients. Thus, small molecules (e.g., nanoparticles) can circumvent the aberrant endothelial barrier and leave the circulation to concentrate at the site of neoplasia. When a high concentration is reached locally, an alternating magnetic field can be used to target the tumour to raise the temperature of the medium.[5,9,63]

The capacity of a material to generate heat under the influence of an AMF is characterized by its specific absorption rate (SAR)[31,52] or specific loss power (SLP), expressed in Wg^{-1} (1.1):

$$\mathrm{SAR} = \mathrm{SLP} = \frac{\Delta \mathrm{T}}{\Delta \mathrm{t}} \frac{\mathrm{C}}{\mathrm{m}_{Fe}} \quad \textbf{(1.1)}$$

where *c* is the heat capacity of the fluid per unit mass, m_{Fe} is the concentration of the colloidal solution studied (g l^{-1} of iron) and $\Delta T/\Delta t$ is the measured temperature increase with time.[52] High values for *SAR* offers the advantages of enable the reduction of MNPs dose, and decrease the values of magnetic field strength and frequency that are required for MHT therapy.

The *SAR* measurement is widely used to characterize the heat generation capability of the system,[10] and it is a crucial parameter to modulate the tissue temperature that will be achieved during hyperthermia treatments. Overheating the tumour may result in serious damage to the surrounding healthy cells or in uncontrolled necrosis. On the contrary, the desired therapeutic effect cannot be achieved if the temperature rise is not high enough.[5] Although this measure cannot be directly compared between different experimental setup's once the SAR value depends on the magnetization - strength and frequency of the used magnetic field[5,52] and on the chemical, physical and magnetic properties of the material. Moreover, it also dependent on the dispersion media and agglomeration degree.[5] The efficiency of power dissipated from SPM particles is enhanced when the particles' size distribution is narrow.[49]

Various factors influence the MHT, the extent of the heating produced and the time during which is maintained the heat as: magnitude of the AMF (the frequency and amplitude); [31,33,42] the size; size distribution and other characteristic of the MNPs,[5,31,40,42,46] the concentration of them in the target place as well the depth of the tumour within the body[31] and the viscosity of surrounding medium.[33,42]

1.2.5.1 Advantages of magnetic hyperthermia treatment

Magnetic hyperthermia (MHT) have a great potential as a stand-alone treatment or adjacent therapy for cancer.[39,52] The first successful clinical trial of interstitial hyperthermia in the treatment of human cancer using magnetic nanoparticles was attempted by Johannsen *et.al*[54] in 2005. Recently, favourable results of the '*nanothermotherapy*' study in Phase II clinical trials run by *MagForce Nanotechnology* (Hospital Charité, Berlin) on patients suffering from

glioblastoma multiform, show an improvement on patient survival from 6.2 to 13.4 months.[52]

The use of SPM NPs prevents the agglomeration of particles in the body, avoiding obstruction of blood vessels.[47] Furthermore, these particles can reside in the body for long time, allowing several heat treatment of the tumour without re-introduction of the MNPs.[15,30]

In addition, as SPM NPs tend to be less than 20 nm and resonate with a magnetic fields ranging from 10 KHz-10 MHz, they can easily penetrate soft tissues and bones.[31] Besides the easiness in penetrating the cells, small particles (< 20 nm) are also more suited for in vivo applications.[12]

MHT is advantageous in treating tumours in organs like lungs, which are easy to locate and avoid thermal bystander effect on nearby regions like heart.[15] Moreover, MHT reaches deeper tissue than any other activation technology (light or acoustic waves).[34] Direct injection to the target tissue allow to put in the target place sufficiently quantities of MNPs to generate the heat needed.[31] MHT cal also be used in conjunction with other treatment modalities of the cancer, such as traditional radiotherapies, like chemotherapy or even surgery, for the purpose of improving the effectiveness of antineoplastic drugs.[36]

The magnetic fluids have a specifically high absorption rate per mass but the normal tissues have a lower absorption rate, so it is possible to selectively excite areas containing fluids without interference with different neighbouring tissues. Such magnetic-field-induced excitation produces heat absorbed mostly by magnetic fluids and thus increasing the temperature only in regions with accumulated magnetic nanoparticles.[14]

MHT has fewer side effects than chemotherapy or radiotherapy[14,64] or anticancer drugs that have to be administered systemically, and with the lack of specificity towards a pathological site, requires a high dose to reach the local in the needed concentration. Moreover, the cancer cells develop resistance to the therapeutic effects of drugs.[15,42] Conventional thermotherapies as photothermal, radiofrequency, infrared or ultrasound exhibit insufficient temperature elevation and non-homogeneity within the tumour[15,42,49] and provides a minimally invasive way to deliver a therapeutic dose of heat specifically to cancerous regions.[49]

1.2.5.2 Disadvantages of magnetic hyperthermia treatment

The inability to precisely control the thermal dose and the dependence of heating efficiency on thermal dose rate is one of the limitations. It is know that large doses of heating can be

achieved by applying large fields amplitudes in a short time frame and result in a more sustained rise in temperature before heat is dissipated,[31] which can provoke discomfort.[15] Non-uniform distribution of nanoparticles throughout the tumour generates cold spots in the regions where no or less MNPs are accumulated, and tumour cells remain untreated in those regions and regrowth occurs subsequently.[15,31] Yet, these cold spots eventually get heated up by active thermal bystander effect. This effect can also heat up normal surrounding cells which need to be avoided; so 3D temperature measurement within the tumour region can help to avoid that situations.[15]

When MNPs are injected intravenously, their biodistribution and achievable temperature is highly dependent on the formulation used, amount of MNPs injected, the target organ and the time point of addition.[15,31] So, the desired heat in the local is complicate to achieved by intravenous administration.[31] In addition, the interaction of MNPs with cells is complex and depending on the physicochemical conditions or the time of exposure, it may also result in the triggering of cytotoxic processes or the internalization of MNPs.[35] Thus, the introduction of the MNPs relied on intratumourally injection, but it is invasive and is not synonymous with uniformity in the introduction of MNPs in the desired place.[31] The optimization process is not yet well understood, experimental results from MNPs systems vary expressively.[52]

The hydrophobic surfaces and the large surface area relative to volume[48,53,58] and therefore possesses high surface energie,[58] MNPs *in vivo* tend to agglomerate and to be released rapidly by the circulation.[17,58,59] Moreover, they tend to have high chemical activity, and are easily oxidized in air (especially magnetite), generally resulting in loss of magnetism and dispersibility.[58] To avoid these difficulties, the surface of the NPs must be modified by a biocompatible polymer.[60,65]

1.2.6. Magnetic nanoparticles in the treatment of cancer

In Table 1.1 are presented some of the nanoparticles used against cancer cells with different types of magnetism.

Table 1.1 -Some examples of different types of NPs used against cancer cells.[39]

Ferrimagnetic	Paramagnetic	Diamagnetic	Antiferromagnetic
iron oxide	palladium	zinc oxide	cobalt oxide
nickel zinc ferrite	cerium oxide	biosynthesized silver	-
magnesium ferrite	titanium dioxide	gold	-
-	platinium	copper	-
-	neodymium oxide	selenium	-

For biomedical applications, MNPs should fulfil a variety of requirements as: (i) SPM behaviour at room temperature, in order to avoid particle aggregation[12,40,45,57] (and escape to induce dangerous thrombosis of blood vessels);[34] (ii) large Ms, so as to show a large response under the application of a magnetic field[40,45,66] and low coercivity (Hc)[49] (iii) limited particle size (<20 nm)[40,66] to escape the phagocytosis of reticuloendothelial system and penetrate into capillary vessels in body tissues, which ensures an effective distribution in specific tissues;[17] (iv) high size unirformity;[45,49] (v) biocompatibility[40,57,65]- nanoparticles are usually coated with either biological or biocompatible molecules;[55] (vii) the carrier particles must have a long retention time while circulating in the blood[40,53] - preventing agglomeration and minimizing adsorption of plasma proteins that enhances phagocytosis (opsonins) on the MNPs by covering them with a thin layer of biodegradable polymer.[40]

1.2.6.1 Why Fe_3O_4?

Fe_3O_4 or γ-Fe_2O_3 (magnetite and maghemite respectively) are the MNPs most used in the research groups and it becomes evident why are attractive candidates for use in human body. Fe_3O_4 is a ferrimagnetic compound with two different cation sites in a unit cell: 8 tetrahedral A sites, and 16 octahedral B sites. Magnetite is an inverse spinel, which means, $(Fe^{+3})[Fe^{+2}Fe^{+3}]O_4$, where the specie in curved parentheses stand for the tetrahedral sites and the square parentheses stand for the octahedral sites.[67]

The iron oxide nanoparticles have good biocompatibility, non-toxicity,[9,28,31,52] potential to exhibit superparamagnetic properties if the particle sized is below 20 nm,[9,28,31] the specific surface is high, biodegradability,[52] high chemical stability[28,31,68] and are excellent conductor

of heating, transmitting it to the adjacent tissues.[31] In addition, the heating efficiency in aqueous colloids of these materials is well established.[69]

Iron is essential in the human body! Besides, it exists in several body entities as in the haemoglobin, which is essential for human survival, it have great stability and unique magnetic properties. Furthermore, iron oxides are not only biocompatible as they can show therapeutic effect, where others nanoparticles as FeSi or FePt fail. Besides, US FDA approve the use of the ultrasmall and/or SPM NPs of iron oxide for MRI (Magnetic resonance imaging)[9,17]. However, it is important to refer the fact that several agents have been removed from the market in the late 1990s and 2000s because the possible side effects. The toxicity is not always immediately detectable.[9]

The surface of the iron oxide MNPs has iron atoms on the surface that can coordinate with molecules or get protonated/deprotonated. This capability allows to modifying the surface pre-and post-synthesis with many functional groups whether inorganic and organic as monomeric ligands (dopamine, phosphoric acid), multimeric ligand and zwitterionic ligand[31,70]; and therefore improve their stability and increase their circulatory halt-time as preventing aggregation, improving their hydrophilic properties and lower the possible cytotoxicity[4,31,70]. The possibility of an easy functionalization[10,33,53] allow obtain a multimode MNP with potential application in several areas.[53]

1.2.6.2 Toxicity

The long terms effects of the MNPs still one the major concerns in their use because of the lack of knowledge of the effect of accumulation of particles in body.[9,71] For example, in blood transfusion, patients suffering for sickle cell anaemia require the constant administration of iron chelating agents in order to control the excess of Fe. Generally, these patients, have reduced life expectancy due to their condition but also due to the iron overload.[9] Landeghem reported in their study that MNPs of iron coated with aminosilanes applied in gliobastoma on phase II were localized in macrophages in areas of tumour necrosis rather than the cancer cells themselves.[72]

Spherical NPs with zwitterionic charged surfaces and hydrodynamic diameter of about 5 nm are released by the kidneys and not entrapped within the reticuloendothelial system (RES) while larger particles (20 nm) are captured by reticuloendothelial macrophages.[31]

Another question, is the time that the iron MNPs can persevere in the body, because they can be uptake by phagocytes cells but also by nonphagocytic cells. For example, the

endothelial cells surrounding the blood vessels, are a sub-group of the latter, and they can engulf the MNPs of iron. Due to oxidative stress, in the case of the γ - Fe_2O_3 uptake, the cells do not survive frequently more than 24 hours post micropinocytosis, and MNPs are cleared through urine rapidly. However, some organs as the lung, liver or kidney have been identified as the main target organs of bioaccumulation of the MNPs in some studies[68,69,71] as well as the macrophages in systemic circulation.[68]

The possibility of these particles to escape from physiological barriers and contact vital organs as the brains is also of high concern.[9]

Nowadays some studies report toxicity to healthy skin and lung tissues *in vitro* tests.[9] However others studies report iron oxide as innocuous to normal rat hepatocytes and human fetal lung cells (IMR-90).[39] These inconsistent results may be due to factors such as dose and exposure duration;[39,68] and MNPs properties and characteristics such as shape, size, charge, biodistribution, functionalizations[39,57,66,69,71] or life cycle[69,71] which influence the results. Further, the behaviour of the MNPs in biological media - the interactions with the cells and tissues can alter the physicochemical properties and contribute in the discrepancy of results of *in vitro* and *in vivo*.[57,69] With a large variety of MNPs and possible behaviours, it is difficult to draw general conclusions about their possible toxicity.[71]

As the possibility of toxic effects are not clear, coating is one of the protective measures to be implemented to minimize iatrogenic complications and damage of healthy tissue.[9] An appropriate coating diminishes systemic toxicity while improving specificity to cancerous cells. However, complete safety is never guaranteed.[9] Also, the MNPs should be tested for microbial contaminations (bacteria, yeast, and mold) eliminating other parameter, which could lead to ambiguous cytotoxic results. The majority of MNPs of iron can be considered sterile due to the synthesis procedures; however, contamination can be introduced in various downstream processes such as surface functionalization.[57]

The consensus at this moment is in favour of their use *in vitro* and *in vivo* experiments involving animals.

1.2.7. Synthesis and coating of MNPs

Various methods of synthesis of magnetic nanoparticles are described in literature.[18] The approaches may be chemical,[5,42,73] biological[42,73] or physical.[5,42] The chemical methods are

the simplest and the most efficient, having a sensible control of composition, shape and size[74] whereas the biological route do not produce homogeneous particles.[74] The physical procedures can be used to produce high purity nanomaterials, but the geometry of the synthesized particles is difficult to control.[45,74] Both methods are able to prepare magnetite with controllable particle diameters, however, well-dispersed aqueous Fe_3O_4 nanoparticles are difficult to achieve.[18] In table 1.2, it is presented some possible methods to synthetize iron MNPs.

The synthesis method has an important role in the magnetic properties[62] as it the size,[33,35,45,62,75] size distribution,[35,62] shape,[45,75] particle surface characteristics,[29,53,62,75] crystalline lattice, oxidation state of iron ions,[53], etc..[42,45,59,62,74]. Various shapes of iron oxides particles such as spheres, cubes, worms, stars, rods, octahedrons, and prism[59] are described in literature.

This work is focus on the use of chemical precipitation to prepare the iron MNPs.

Table 1.2 -Summary of some synthetic methods of magnetic nanoparticles.

Methods		Ref.
Chemical	co-precipitation	5,18,35,53,73
	thermal decomposition	5,18,29,35,53
	microemulsion	18,29,35,53
	hydrothermal synthesis	5,53,76
	microwave assisted synthesis	73
	solvothermal method	45,73
	self-assembly	60
	combustion synthesis	73
	sol–gel	73
	polyol method	5
Physical	Gas phase deposition,	5,50
	ball milling	5,50
	laser-induced pyrolysis	5,45,50
	electrodeposition	45
	pulsed laser ablation	45,50
	aerosol	45,50
Biological	magnetotactic bacteria	73
	mediated by proteins	50,53
	mediated by fungus	50

1.2.7.1 Chemical Precipitation

Co-precipitation of ferrous and ferric salts in aqueous solution represents a straightforward, facile and efficient synthesis strategy to synthetize iron oxide NPs on a large scale.[70] A wide variety of experimental parameters, such as: i) pH; ii) ionic strength; iii) concentrations ratios of Fe^{2+}/Fe^{3+}; type of precipitation agent; v) strength of the basic agent;[5,45,70] vi) reaction temperature;[5,18,45,53,70] and vii) stirring rate[5,18,45,47,53] were described in the literature that influence size, shape, magnetic and surface properties of the MNP synthetized. For example, if the concentration of the salts is enlarged, there is an increase in the number of particles, with a subsequent loss of uniformity in size.[5,45,53] However, the control of the particle size distribution, crystallinity and oxidation is limited once the reactions are thermodynamically driven.[13,47,70] This could be overcome by others alternatives as thermal decomposition. However, the MNPs synthetized by this method generally are non-aqueous, being soluble only in organic solvents. Post-preparative ligand-exchange procedures are require to turn the particle water-soluble and biocompatible.[70]

The precursors used are ferric (Fe^{3+}) and ferrous (Fe^{2+}) chlorides, sulphates, perchlorates or nitrates, etc..[5,45,76] They are, first dissolved in an acidic aqueous solution to prevent the individual precipitation of hydroxides whose solubility products are very high. Then they are "co-precipitated" (meaning the two valences of iron ions together) under the addition of a strong base (commonly NaOH), according to the reaction 1.2.[5,13,45,53] It is not needed high temperatures[18,76] and the resulting particles surface possesses hydrophilic properties. Also, it can produce fine, high-purity, stoichiometric particles of single and multicomponent metal oxides.[35]

$$2\ Fe^{3+} + \ Fe^{2+} + 8\ OH^- \rightarrow Fe_3O_4 + 4\ H_2O \qquad \textbf{(1.2)}$$

Controlling the reaction atmosphere is also of crucial importance in this method, since - magnetite (Fe_3O_4) easily oxides into maghemite (γ-Fe_2O_3), a ferrimagnetic iron oxide phase or hematite (α-Fe_2O_3), a antiferromagnetic iron oxide. Therefore, inert conditions are required to obtain magnetite, or a controlled oxygen atmosphere.[5,45,53] For example, bubbling the solution with an inert gas does not only protect the critical oxidation of magnetite, but also reduces particle size when compared with methods that do not remove oxygen.

1.2.7.2 Geometry and Size

The geometry and size of the MNPs are important to define their lasting time in the bloodstream. Rapid removal of them from circulation systems by opsonins or white cells can substantially reduce their biomedical functionality. The dimensions of the MNPs directly influence their trajectory in the body. MNPs larger than 100 nm are usually opsonized[63] and if lower than 5-6 mm diameter are removed by renal filtration.[77] In general, the larger the particle, the lower their spent time in blood circulation. Thus, it is commonly accepted that MNPs with a diameter of between 1 and 100 nm are the most suitable for *in vivo* application.[63]

Spherical MNPs have been the most studied form. They are isotropic whereas the elongated MNPs, exhibit magnetic shape anisotropy. The magnetic shape anisotropy is a property that reflects the existence of a preferential direction magnetization dependent of the particle shape, being an advantage.[63] The magnetic moments of spherical nanoparticles are arranged in a random way, and tend to cancel, diminishing the strength of the magnetic signal. In anisotropic MNPs, the magnetic moments tend to orient themselves according to their long axis and they will always be pointed to two possible ways, in the same direction. Thus, the strength of the magnetic signal is enhanced, i.e., elongated particles experience a greater strength when compared to spherical particles of the same volume.[63]

1.2.7.3 Surface modification of iron oxide MNPs

As MNPs usually tend to aggregate,[15,33,35,45] the coating of synthesized MNPs is advised.[33,45] Furthermore, the naked MNPs can stimulate ROS generation and non-specific interactions with opsonins[5,10,33,53] (albumin, immunoglobulin (IgG), apolipoproteins, etc.), which adsorb onto the MNP surface, thereby completely obstructing their functionality and allowing their uptake by the phagocytes of the immune system (IS)[5,33,53] which results in increased cytotoxicity.[45]

As the microenvironment where the cancer cells are developed are hostiles (acid medium, low oxygen) the surface modifications must take that in account.[45,53] For example, if the intend is reduce the adsorption of MNPs by the opsonins, they may be coating with amphiphilic molecules and then increase the time in blood circulation.[33]

The interaction between the coating agent and the MNPs is critical[35,45] and the special attention must be taken to insure the stability of the MNPs. For example, physically adsorbed coatings (by electrostatic interactions or hydrogen binding) show limited stability in comparison to chemically adsorbed coatings agents. The steadiness of the coating also depends on the quantity of the chemical interaction that each molecule or macromolecule can establish with the MNPs surface.[13]

The goal stands by offering a non-toxic[35,48] and biocompatible coating[5,35,45,47,62] so that the crystalline character of the oxide is retained[33,53,62] as well increase the chemical stability of the Fe_3O_4 NPs[5,10,17,18,35,44,45,48,53] *in vivo*. Further, the route employed should be simplistic and effortlessly.[62]

A variety of materials have been reported to coating the Fe_3O_4 MNPs. Some are presented in table 2.3.

In this work, it was tried to synthesize magnetic NPs of iron oxide, coated with biocompatible and non-toxic chitosan biopolymer.

Table 1.3 - Some materials reported as coating/crosslinkers and linkers to the iron oxide (Fe_3O_4).

Coating	Examples	Ref.	Examples	Ref.	Examples	Ref
Organic molecules	oleic acid	17,35,78,79	castor oil	30	oleylamine	80
	phosphates	54	nitrilotriacetic acid	81	dimercaptosuccinic acid	71
	Gallic acid	75	gluconic acid	82	Carbon	83
	Caffeic acid	84,85	lactobionic acid	82	RHGD cyclic peptide	86
	dopamine	81,87	polyacrylic acid	82	hyaluronic acid	88
	dopamine sulfonate	89	folic acid	15,47,90,91	HEMAGl	92
	citric acid	93,94	iminodiacetic acid	16	sodium hyaluronate	87
	acid carboxyl	95				
Polymers	Dextran	15	gelatin	65	methacrylamide	92
	Starch	96	chitosan	12,16,18,30,40,44,48,65,73,96–102	fucan polysaccharides	103
	Alginate	104	o-carboxymethyl chitosan	14	chitosan-L-glutamic acid	41
	pullulan	105				
	aminosilane	106,107	polystyrene	78	Pluronic® block copolymer	108
	PEG	71,88,109–111	PNIPA	12		
Inorganic Materials	Au	112	alkosilanes	78,113–1151	silica	44
	Ag	117	silicone	118	Si	119

1.2.7.4 Chitosan

Chitosan is a biopolymer with a unique chemical structure, high density, free amino and hydroxyl groups[120] and easy application.[62] Amongst the biocompatible natural materials employed as coatings, chitosan has been used due to its known properties as: biocompatibility, biodegradability,[17,40,44,120–122] bioactivity,[18,29,122] hydrophilicity (provides a barrier to adsorption of protein, reducing the macrophage),[30,44,123] bioadhesion,[17,73] low cytotoxicity,[15,16,18,30,120] antioxidant, anti-inflammatory[120] and antimicrobial properties.[16,120] Chitosan have been used for various biomedical applications such as tissue engineering, drug delivery,[15,65] cell encapsulation, wound healing along with orthopaedic, periodontal, pharmaceutical and gene therapy[65] among others.

Chitosan or poly[β-(1-4)-2-amino-2-deoxy-D-glucopyranose], is obtained by partial alkaline deacetylation of chitin[15,29,120] (about >50%), a main component of the exoskeleton of crustacean, mollusc shells, fungal cell walls and insect cuticles.[18,65,120] Their structure is very similar to that of cellulose[120,124] and is characterized by their molecular weight and degree of acetylation,[120] which are determinant on various properties including solubility, biodegradability, toxicity, antimicrobial activity, etc.[124] This biopolymer has a positive charge, being soluble in various acids.[100]

In addition, the free amino groups and hydroxyl groups can be easily used for further functionalization[17,33,40,44,73,121] and improve the colloidal stability *in vivo* in blood circulation.[17,122] But chitosan cannot dissolve in a physiological environment (pH = 7.4), only in acidic solution (pH < 6),[15,120] where the units of glucosamine ($-NH_2$) can be converted into their protonated and soluble form (NH_3^+).[120,124] This is the main disadvantage of coating the MNPs with chitosan because can interact with anionic components (glycosaminoglycans and proteins).[125] But, *Nunes et al.*, demonstrated that chitosan can link to genipin and caffeic acid molecules, becoming less soluble in acid medium between chitosan chains.[126] Based on this result, there is a way to make chitosan more stable in acidic medium. So, the main disadvantage of chitosan can be overcome.

1.3 Motivation

As everything it is used inside of human body, biocompatibility is required. More, in the case of the MNPs, to achieve better results in the heat generated, disaggregation is need. So, coating is a possible method to achieve these two requirements, for the use of the MNPs in hyperthermia therapy. Promote a good link between the iron oxide and the coat is fundamental, so adversely effects are avoiding as well to achieve better heat production during the hyperthermia treatment.

In the beginning of this work dopamine never was used to promote this type of bonding (between iron oxide and chitosan) in this type of therapeutic (magnetic hyperthermia). Tumour cells are more acid and chitosan have poor resistance to acid medium. To overcome this issue, crosslink with a known molecule is proposed: genipin. Due to structural similarity with dopamine, caffeic acid was proposed to see if could promote a good link between the iron oxide as well to see of the link to the coat is stronger than using dopamine and genipin.

1.4 Objectives

The general objective of this work was to prepare suitable magnetic nanoparticles to be used in magnetic hyperthermia.

To reach the main purpose of this thesis, it was necessary accomplish minor objectives:

- To produce magnetic nanoparticles (MNPs) of iron oxide, preferably magnetite superparamagnetic NPs;
- To functionalize the produced nanoparticles through two different ways: one using dopamine (DOPA) and the other using caffeic acid (CA);
- To coat the nanoparticles with chitosan;
- To characterize structural and morphologically the NPs through different techniques as X-ray diffraction (DRX), Fourier transmission infrared spectroscopy (FTIR), transmission electronic microscopy (TEM), Zeta Potential and hydrodynamic diameter (DLS) and to evaluate the magnetic properties after the coat of chitosan by Superconducting Quantum Interference Device (SQUID);
- To perform hyperthermia measurement of the produced MNPs.

EXPERIMENTAL PROCEDURE

Experimental Procedure

This chapter describes, briefly, the materials and procedures used, as well as the characterization techniques. The reagents used were commercially available and used without pre-treatment. The main characteristics of all reagents used are in Annex A. To avoid the production of impurities was used Type 1 water from Millipore Simplicity UV Water Purification System.

Figure 2.1 represent the main steps of this experimental work.

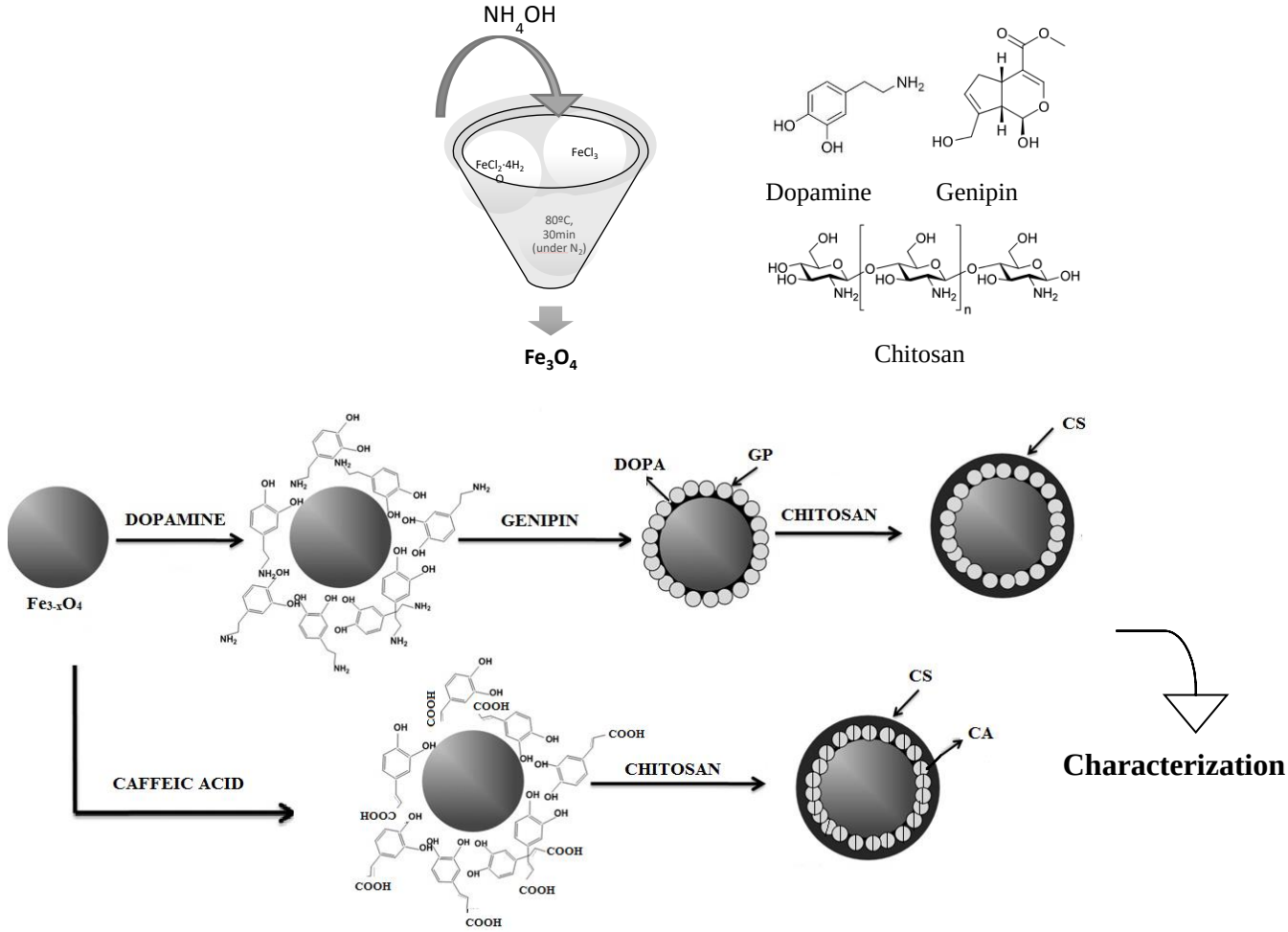

Figure 2.1 Schematic representation of the main steps during laboratorial work. In top, the synthesis of Fe_3O_4 and down, the paths for the functionalization and coating.

It is divided in four parts: i) synthesis of iron oxide MNPs; ii) functionalization and coating of the MNPs synthesized; iii) morphological, structural and magnetic characterization and iv) magnetic hyperthermia measurement (based on the release heat by the NPs).

2.1 Synthesis of iron oxide MNPs

The synthesis of the iron oxide MNPs was adapted from the chemical co-precipitation method described on reference (78). The experimental apparatus used in the synthesis is shown in Figure 2.2. The reagent quantities used in the synthesis of MNPs are presented in Table 2.1.

Figure 2.2 Experimental apparatus used for synthesis of NPs of MNPs.

Table 2.1 Reagent quantities used in the synthesis of MNPs.

	$FeCl_2 \cdot 4H_2O$	**$FeCl_3$**	**Fe^{3+}/Fe^{2+}**
Mass (g)	7,2021	4,98	-
Molar quantity (mol)	0,0444	0,0250	Ratio=1,76

Briefly, the MNPs were produced by co-dissolving $FeCl_3$ and $FeCl_2 \cdot 4H_2O$ in 50 mL of water under nitrogen gas with vigorous stirring at 80ºC. Then, at this temperature, 25 mL of ammonium hydroxide were rapidly added into the solution. The solution immediately turned black. The solution was kept reacting at 80ºC for 30 minutes and cool down to room

temperature. To get particles free from sodium and chloride compounds, the MNPs were magnetically separated and washed with water. This procedure was repeated three times, and then MPNs were dispersed in 72 mL of water. The pH of the suspension of NPs was neutral.

2.2 Procedures for coating of MNPs

2.2.1 Functionalization of the MNPs with dopamine

Dopamine was used as the anchor to present functional molecules on the surface of iron oxide magnetic nanoparticles. Adapting the procedure of (81), dopamine (38.00 mg) was dissolved in 14 mL of water and ethanol (2.5:1). The functionalization was made by mixing 5 mL of iron oxide (dropwise) to dopamine solution under using an ultrasound bath for homogeneizing. After, the pH was adjusted to 4-5 (4.57) with HCl (1 M). The resulting black solution was put in the ultrasound for 20 min. The MNPs were magnetically separated and washed with hexane. This process was repeated three times. The MPNs functionalized with dopamine were dispersed in 22 mL of ethanol and denoted as F.DOPA.

2.2.2 Addition of genipin molecule as “tethering” agent

Genipin molecule was reacted with dopamine to act as bridging ligand to chitosan.
The addition of genipin to the functionalized dopamine’s iron oxide was made in the proportion of 1:2. 30.1 mg of genipin, was dissolved in 20 mL of ethanol followed by 5 min in the ultrasound. 4.8 mL of F.DOPA suspension were diluted in 20 mL of water:ethanol (2:3). The functionalized iron oxide was dropped to the genipin solution under ultrasound and left reacting overnight in the dark. Afterward, the MNPs were centrifuged twice at 6000 rpm during 90 min and then the pellet powders were ressuspended in isopropyl alcohol. Lastly, the MNPs were magnetically separated and suspended in 30 mL of ethanol, designated as F.DOPA.GP.

2.2.3 Functionalization of the MNPs with caffeic acid

Adapting the procedure of functionalization with dopamine of reference 81, 36.10 mg of caffeic acid (CA) was dissolved in a mixture of water and ethanol on the molar ratio of l2.5:1. Then 5 mL of iron oxide was added dropwise to the CA solution under ultrasound. After, the pH was adjusted to 4-5 (4.46) with HCl (1 M) and then, the black solution was ultrasonicated for 20 min. Lastly, the NPs were separated magnetically and wash 3three times with ethanol, and redispersed in 40 mL of ethanol. These particles were designed FCA.

2.2.4 Coating of the functionalized MNPs with chitosan

A chitosan solution (CS) was prepared with the concentration of 1.5% (w/v) in 0.1 M acetic acid and was stirred over night at room temperature. After complete dissolution of chitosan, the solution was filtered in a glass fritted funnel (G1).

Despite knowing that coating isolated MNPs is extremely hard as well as getting them homogeneously coated with similar coating thickness, it was that the starting point to determine the amount of chitosan to add to the samples. So, it was estimated the average particle diameter as well as total volume of the coating and multiplied by the total estimated number of particles present in the volume of solution to be coated.

2.2.4.1 Coating of F.DOPA.GP with chitosan

303 µL of 1.5% (w/v) chitosan solution that was diluted in 20 mL of water under ultrasound. 4 mL of the F.DOPA.GP were dropwise to the chitosan solution under ultrasound. This step takes almost 40 min. The mixtures were left reacting in the dark at room temperature for 48 h. After, the NPs were magnetically separated and washed three times with water and resuspended in 3 mL of water.

In order to optimize the coating, the same amount of CS was added to a smaller amount of MNPs. Thus, 303 µL of CS was diluted in 20 mL of water under ultrasound and 1 mL of F.DOPA.GP was dropwise to the chitosan solution. The following steps are equal to those above. This was the solution that was characterized.

2.2.4.2 Coating of F.CA NPs with chitosan

To caffeic acid nanoparticles with chitosan two paths were followed. The first one was based on the procedure reported in the reference (126) and the second was based on the reaction of the carboxylic acid group of the caffeic acid with the amino groups of chitosan using carbodiimide chemistry.

2.2.4.3 Coating of F.CA with chitosan using ceric ammonium nitrate

3.17 mL of CS was dissolved in 209 mL of water under ultrasound. Ceric ammonium nitrate CAN (0.1048 g) was dissolved in 3.17 mL of water. 2.72 mL of F.CA was added to the previous solution. Under nitrogen gas, FCA-CAN was added under ultrasound to the CS solution protected from light and left to react always under ultrasound during 3 hours. The orange solution was separated magnetically and ressuspended with water. The suspension was centrifuged six times for periods of 30 min at 6000 rpm. Lastly the NPs were lefted in 26 mL of water (Figure 2.3).

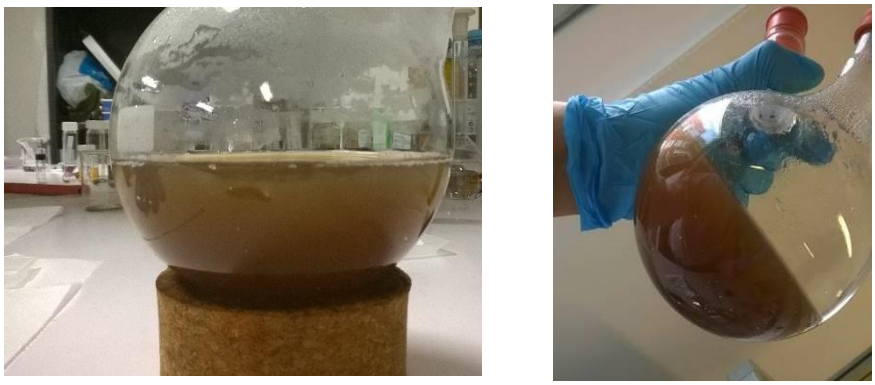

Figure 2.3 Final aspect after coating the MNPs with chitosan via CAN.

2.2.4.4 Coating of F.CA with chitosan via 1-Ethyl-3-(3-dimethylaminopropyl)carbodiimide

FCA NPs were magnetically separated and ressuspended in the same volume with 2-(*N*-morpholino)ethanesulfonic acid (MES) buffer (pH 5.5) to avoid irreversible oxidation of catechol group of caffeic acid. 1-Ethyl-3-(3-dimethylaminopropyl)carbodiimide (EDAC) was added to the FCA solution immersed in a ultrasound bath for homogeneization (in cold water) and stirred at room temperature overnight, at 25 rpm and at 360º in a PTR-35 360° vertical multi-function rotator from Thomas Scientific. The FCA solution was dropwise to

the CS solution (2 mL of the 1.5% m/v diluted in 15 mL of water and at pH≈2.5) under ultrasound and put again in the rotator to stirred for 24 h. After, the MNPs were magnetically separated twice and washed with water and ressuspended in 5 mL of water. The stoichiometric molar ratio of FCA and EDAC was 1:7.5. The MNPs was designated EDAC.

2.3 Characterization of the NPs

2.3.1 Structural and morphological characterization

2.3.1.1 X-ray diffraction

X-rays diffraction (XRD) is a very useful technique aiding qualitative and quantitative analysis on the crystalline structure and particle size.[127,128] X-ray techniques are generally non-destructive and allow information about the ensemble average of many particles in contrast to direct imaging techniques such as electron microscopy that only gives data concerning a small part of the sample. This data that may not be truly representative of the material.[128] Exposing a sample to X-rays beam, some of those X-rays are diffracted according to a certain angle (2θ) matching characteristics crystallographic directions of the material as given by the "Bragg's law":

$$n\lambda = 2d\sin\theta \qquad \text{(Eq. 2.1)}$$

where λ is the wavelength of X-rays source, θ is the angle between the incident waves and the crystal surface, and d is the spacing between the crystallographic planes of the crystal.[129] The obtained MNPs were dried at 60 ºC overnight and left cool to room temperature in a desiccator before characterization by XRD.

The analysis was performed in a diffractometer of powders Panalytical Empyrean, using Gonio as a scan axis, Cu radiation, λ=1.54056 Å, at 40 mA, 45 kV, with a range of 15º - 100º and a step of 0.013º. Data acquisition was done automatically using the software Identification and Crystallite size calculator – high Score Plus from Panalytical, between 15 and 99° (2θ). The peak identification was made using the data base from The International

Centre for Diffraction Data (ICDD), PDF 4+ (2015). The Rietveld refinement was made using a GOF of 1.509.

2.3.1.2 Fourier transformed infrared spectroscopy

The MNPs synthetized as some reagents were analysed by Fourier transformed infrared spectroscopy (FTIR) technique, in order to identify the characteristic vibration between atoms presents in the samples, helping to identify specially the organic functional groups of the coating species.

The samples analysis was performed on a Mattson Instruments, GALAXY SERIES FT-IR 7000, for an infrared region of 4000-350 $cm^{-1,}$ with a step resolution of 4 cm^{-1} and a background scan of 256. The sample was analysed in ATR mode.

2.3.1.3 Thermogravimetric Analysis (TGA)

TGA provides quantitative evidence of the thermal stability of the samples, allowing to determine the amount of organic content present on the MNPs. This is an tremendously valuable technique for surface characterization on MNPs and to understand the success of the coating reaction.[17]

The weight variations with temperature were performance in a *Setaram* model *Labsys™ TG-DDSC16*. This technique provides information about the transformation that is occurring by overlapping the weight loss curve as a function of temperature. The NPs of magnetite were dried at 60 ºC during 12 h and milled in a mortar before. The analyses were done by heating the powder from room temperature to 600 ºC at rate of 10 ºC/min under flowing air.

2.3.1.4 Transmission Electron Microscopy (TEM)

The morphology and size distribution of the MNPs before and after were studied by using transmission electron microscopy. A *Hitachi®* model *H9000* with an acceleration voltage of 300 Kv microscope was used for the analyses.. The sample were dispersed in ethanol and stirred in ultrasound for 30 minutes. The samples were prepared by dropping the suspensions on a copper grid coated with an amorphous carbon film.

2.3.1.5 Hydrodynamic Size (DLS) and Zeta Potential

Hydrodynamic particle sizes were measured by Dynamic Light Scattering (DLS)[130] that can provide information about the size and size distribution in suspensions in a short time.[11] A cuvette containing the sample is irradiated by a polarized laser beam, which leads to a scattering signal in all directions, depending on the particle size. Once the particles are suspended within a liquid, undergo Brownian motion and these movements induces temporal variations of the scattered intensity recorded at a given angle. The larger the particle, the slower is the browninan motion. The time Auto-Correlation Function (ACF) of the intensity signal is analysed to obtain the Particle Size Distribution (PSD).[130] DLS is very sensitive to the quality of dispersion, degree of aggregation of the NPs and stability of the suspensions, that can create misleading results.[11]

The particle hydrodynamic size, as well as the Zeta Potential were measured by a Malvern Zetasizer Nano ZS™. For DLS measurements water was used as the dispersion medium at 25ªC using plastic cells with a detection angle of scattered light at 173º. The samples were diluted to a concentration of 5.0×10^{-4} g/L and stirred for 5 minutes.

The isoelectric point of pure and coated samples and additional information about the coating of nanoparticles were obtained using the measurements of electrophoretic mobility's.

The ζ-potential was measured by electrophoretic measurements in a 0.01 M KCL solution. To change the pH of the suspensions in DLS and ζ-potential measurements NaOH and HCl were used.

2.3.2 Magnetic Characterization

Superconductor Quantum Interference Device (SQUID) magnetometers was used to measure the magnetic properties of the sample iron oxide nanoparticles before and after coating. In a SQUID magnetometer, the samples moved through the external magnetic field. The magnetization measurements were performed as a function of temperature between 10K and 390K under an applied magnetic field of 50 Oe. The ZFC (Zero Field Cooling) curves were obtained after cooling in Zero Field, from room temperature. The FC (Field Cooling) curves were obtained after cooling in the measurement field. The magnetization curves as a function of applied magnetic field were performed at 300 K varying the pitch

between -55 and +55 kOe. These measurements were performed in a *Quantum Design-MPMS* magnetometer from *Centro de Física Matérica Condensada- Faculdade de Ciências* from University of Lisbon.

2.3.3 Magnetic hyperthermia measurements

A more effective way to destroy cancer cells is to use the nanoparticles as little magnetically driven drill bits. Through a pair of Helmholtz coils arranged perpendicularly it is possible, in a simple way, to generate rotating magnetic fields that are few millitesla. However, it is necessary a system of cooling because increasing the magnetic field beyond this point can result in resistive heating due the continuous current[131].

The measurements were made in an equipment consisting by a power source (EASYHeat 0224 FF CE, *Ambrell*), a Helmholtz coil with two twists, a cooling system (Chilly 25-S HYFRA) and an optical pyrometer FTP LN2 (sensor - FLUOTEMP Fiber Optical Temperature Sensor System). The determination of specific absorption rate (SAR) was based on the obtained results in measurements of heat release of the samples, when subjected to an external magnetic field of alternating current.

The measurements were made in an Ambrell jar, where 3 mg of the test sample were dispersed in 3 mL of ethanol and, similarly, a sodium citrate solution (5%). To disperse the MNPs the samples were stirred for one hour in. The container was then placed inside the cork holder which was among the coils of the Helmholtz coil. The alternating current magnetic field was applied for 5 min using the following parameters: a current (*I*) 400 and the frequency (*f*) at 275 kHz. Under these conditions the maximum magnetic field applied alternating value will be ≈ 120 Oe.

RESULTS AND DISCUSSION

Results and Discussion

The main goal of this work was to synthesize magnetic nanoparticles (MNPs) with applicability in magnetic hyperthermia through introduction of news groups (the ligands agents). For the reasons given above, the chosen MNPs to synthetize was magnetite, due to their properties as biocompatibility, strong magnetization, low toxicity among others reported here and in a large bibliography over the last years.

There are many ways to synthesize NPs of magnetite. The methods pass by thermal decomposition, chemical co-precipitation, hydrothermal technique, electrochemical synthesis, ultrasound[132] among other already mentioned in this work. But, the chemical precipitation is the most widely used synthesis procedure, both for laboratory scale and for industrial use.[133] The reasons for the popularity of the chemical precipitation are the low temperature of reaction; the easiness and low cost,[100,133,134] conjugated with the harmless and biocompatible reagents, which make the resultant MNPs suitable for biomedical applications once produces NPs in aqueous phase with a no impurities.[100,133]

3.1. Synthesis of iron oxide MNPs

Alkaline chemical precipitation was used to synthesize iron oxide MNPs. The chemical reaction of this synthesis is present in reaction 1 of the Table 3.1. To provide a complete precipitation of the used iron salts and avoid oxidation of magnetite, a high pH was required,[105,135] as well as N_2 atmosphere. Bubbling nitrogen gas through the solution not only protects from oxidation but also reduces the particle size when compared to others methods in the presence of oxygen.[105] The low temperature used (80 ºC) was higher enough to prevent the production of iron oxide-hydroxide ($FeO(OH)\cdot nH_2O$) that can be easily converted to γ-Fe_2O_3 (maghemite). 80 ºC is low reaction temperature when compared to another methods such as thermal decomposition, solvothermal or hydrothermal synthesis.[135]

Table 3.1 Possible oxidations reaction that may occur in aqueous solution when iron (II) and (III) are present[136].

	Reaction	Phase
(01)	$Fe^{2+} + 2Fe^{3+} + 8OH^{-} \rightarrow Fe_3O_4 + 4H_2O$	Magnetite
(02)	$2Fe_3O_4 + ½\ O_2 \rightarrow 3\ \gamma\text{-}Fe_2O_3$	Maghemite
(03)	$2Fe^{3+} + 6OH^{-} \rightarrow \gamma\text{-}Fe_2O_3 + 3H_2O$	
(04)	$2Fe(H_2O)_6^{3+} \rightarrow \alpha\text{-}Fe_2O_3 + 6H+ + 9H_2O$	Hematite
(05)	$Fe_3O_4 + ¼\ O_2 + 9/2\ H_2O \rightarrow 3Fe(OH)_3$	Hydroxide de Fe (III)
(06)	$Fe^{3+} + 3OH^{-} \rightarrow Fe(OH)_3$	
(07)	$Fe^{3+} + 3OH^{-} \rightarrow \alpha\text{-}FeOOH + H_2O$	Goethite
(8)	$Fe^{3+} + 2H_2O \rightarrow \alpha\text{-}FeOOH + 3H^{+}$	
(9)	$Fe^{2+} + ¼\ O2 + ½\ H_2O \rightarrow Fe^{3+} + OH^{-}$	Oxidation de Fe^{2+} para Fe^{3+}

The alkalization of the reaction was carried out through the addition, in excess, of a weak base (NH_4OH) instead of a strong base such as NaOH. The weak base provides a stable concentration of OH^- in the whole reaction instead of high concentration of OH^- in the beginning of the reaction.[83] Because of the constant concentration of the OH^- in the solution, the solution is far from the isoelectric point, which is at pH 3.5, (Figure 3.17). So, the electrostatic forces between growing particles prevent their aggregation and the resulting particles are smaller,[137] with a higher crystallinity and saturation magnetization (*Ms*) than if it was used a strong base.[83] So, the use of a surfactant during their synthesis to make the particles away from each other is not really needed with this method. However, after the synthesis, the need to remove the chlorides and ammonia ions from the solution made by washing the NPs with water, which neutralizes and approached the pH of the solution to the isoelectric point, thereby facilitating the aggregation of them.

The produced NPs are presented in Figure 3.1. The black colour suspensions settle in a relative short time, which demonstrates the high degree of aggregation of the NPs (which was later confirmed by TEM, in Figure 3.5. The magnetic behaviour of the particles was tested initially with the help of a permanent magnet. (Figure 3.1b). As it possible to see, the particles strongly are strongly attracted to the magnet, but soon as the magnet was removed, it was observed that the particles recovered their initial properties.

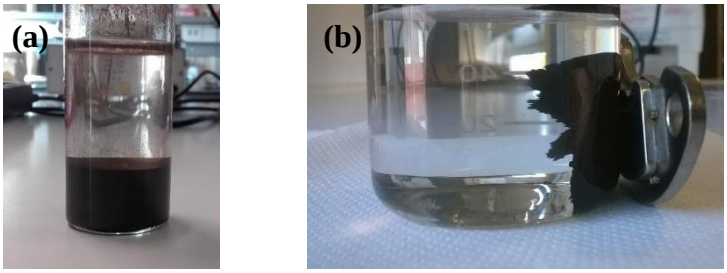

Figure 3.1 (a) Image showing the response of the produced MNPs in the absence of magnetic field (B=0) and (b) in the presence of magnetic field (B>0).

Although chemical precipitation is a facile and rapid method of synthesis, magnetite have low stability in aqueous medium.[100] Due to the oxygen present in the water, is able to be oxidized leading to the formation of other iron oxide like maghemite, goethite or iron hydroxide (III)[136] (Table 3.1). After 8 months reserved in water, the same MNPs once had black colour, now shows a brownish colour, characteristic of one of other possible iron oxide: the maghemite. In Figure 3.2, it is possible to see the change in colour of fresh synthesized iron oxide NPs, with black colour (a) designated as Fresh NPs, and after eight months aging, designated Old NPs (b), with a brownish colour. This change in colour is due to the oxidation.

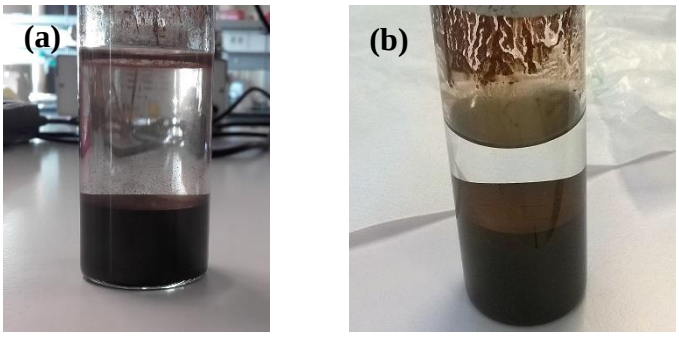

Figure 3.2 Experimental appearance of iron oxide MNPs: (a) Fresh MNPs; (b) Old MNPs after 8 months of aging.

The Rietveld refinement of Fresh and Old NPs is presented in Figure 3.3. The main peaks are observed to match with the Bragg reflection planes of the cubic crystal structure of magnetite which is confirmed by JCPDS card no.: 88–0315. In the case of Old particles more than one phase was found, as it was suspected from the brownish colour. The phases that were identified were magnetite and iron hydroxide (III).

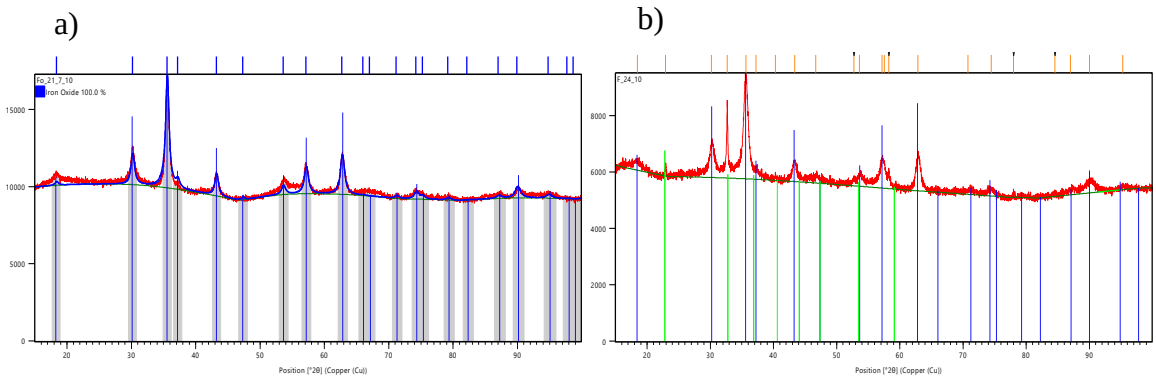

Figure 3.3 Results of the Rietveld refinement of the X-ray diffraction patterns for synthetized iron oxide MNPs: (a) Fresh NPs, where the blue line represents the Bragg position; (b) Old NPs where orange line represents the Bragg position of two phases: magnetite (blue) and iron hydroxide (green).

The easiness of oxidation of the magnetite NPs makes very difficult to synthesize and stabilize pure magnetite,[54,82,138] being in most of the cases, a mixture of magnetite and maghemite that is obtained.[138] Mössbauer spectroscopy is the only technique, which could identify the crystalline phase composition of different iron oxides. But it was not possible to collect this data. Then, when the refinement says it is only present one phase and corresponds to the magnetite phase, it is possible that this is not true. For example, the standard diffraction pattern for magnetite (JCPDF 01-088-0315) and maghemite (JCPDF 00-039-1346) powders are compared in Table 3.2. They are very similar, with maghemite values slightly higher than magnetite, demonstrating the difficulty to distinguish between two similar phases like as magnetite and maghemite. Both of them have spinel structure with very closely Bragg position. From the comparison between the Old and Fresh NPs with the provided JCPDF data, it is possible to see that both NPs have 2-θ values closer to the JCPDF of magnetite than to maghemite. This may indicate that magnetite is present in both, and in greater quantity than maghemite, but still, is just a qualitative information. Other techniques as FTIR and TGA were be performed to strength this information once the only technique could not be performed.

The average crystallite size was determined by the Scherer's equation (3.1):[139]

$$\tau = \frac{K\lambda}{\beta\cos(\theta)} \qquad \textbf{(3.1)}$$

where K is the grain shape factor, λ is the incident X-ray wavelength, β is the full width at half-maximum (in radians) of the highest intensity peaks (311) and θ is the corresponding diffraction angle. Fresh NPs have average particle size of 14.7 nm and Old NPs have 11.2 nm, which is in agreement with results published in literature.[133] Both NPs are below the

critical size for SPM NPs (<20 nm). The broadness of the reflexion peaks (full width at half maximum) of the X-ray diffractograms is indicative of the nanometer size of the synthesized NPs (Figure S1 in annex).

The size of the MNPs developed in this study is suitable for medical applications.

Table 3.2 Position of the main diffraction peaks of the synthesized Old and Fresh MNPs and comparison to the data found in the JCPDF database concerning magnetite (Fe_3O_4) and maghemite (γ-Fe_2O_3).[138]

Old		**Fresh**		**Fe_3O_4 01-088-0315**		**γ-Fe_2O_3 00-039-1346**	**Old**		**Fresh**		**(h k l)**
2-θ	I(f)	2-θ	I(f)	2-θ	I(f)	2-θ	Fe_3O_4	Fe_2O_3	Fe_3O_4	Fe_2O_3	
30.18	43.24	30.06	37.05	30.16	28.8	30.24	0.02	0.06	0.10	0.18	(2 2 0)
35.46	100	35.50	100	35.52	100.0	35.63	0.06	0.17	0.02	0.13	(3 1 1)
37.12	21.62	37.07	16.39	37.16	7.9	37.25	0.04	0.13	0.09	0.18	(2 2 2)
43.10	31.35	43.16	30.49	43.17	20.7	43.28	0.07	0.18	0.01	0.12	(4 0 0)
53.70	23.24	53.54	17.38	53.56	8.7	53.73	0.14	0.03	0.02	0.19	(4 2 2)
57.18	44.86	56.98	31.75	57.10	28.7	57.27	0.08	0.09	0.12	0.29	(5 1 1)
62.78	62.16	62.48	41.97	62.70	37.1	62.92	0.08	0.14	0.22	0.44	(4 4 0)

FTIR measurements were performed to check the chemical bonds in the as-synthesised and functionalized MNPs. The spectra of Figure 3.4 shows that Old and Fresh NPs are composed of three characteristic bands: a broad band between 3000-3500 cm^{-1} related to the -OH stretching vibration modes of water, a band at ~1630 cm^{-1} attributed to the O-H stretching vibration mode and a band at ~530 cm^{-1} which is characteristic of the Fe-O stretching vibration.[41,73,100] By analysing comparably the FTIR spectra of Old and Fresh MNPs (Figure 3.4), it is possible to suspect that the Old MNPs consist in a mixture of magnetite and maghemite, since the band located at 528 cm^{-1} is not as sharp as the one displayed by the Fresh MNPs, which should be mainly formed by magnetite.[138]

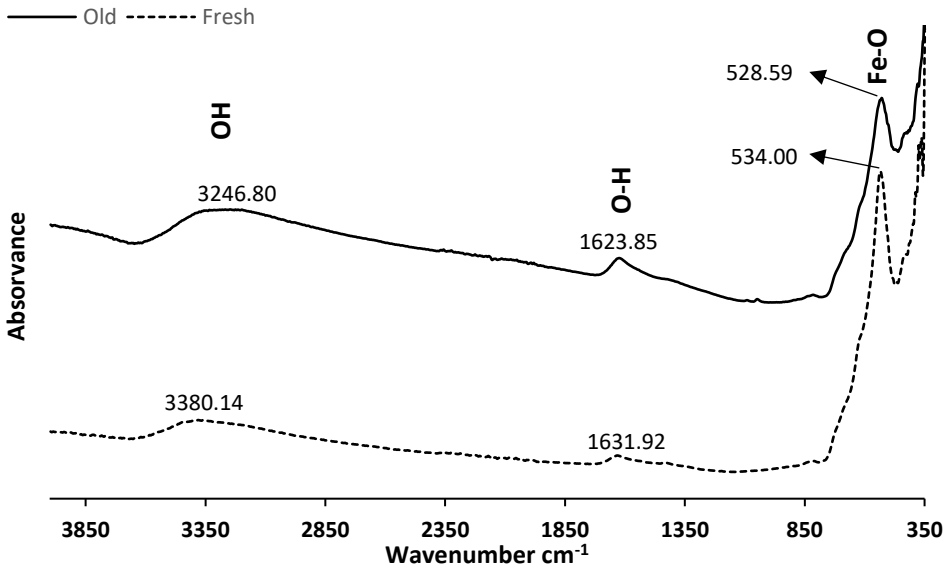

Figure 3.4 FTIR spectra of Old (continuous line) and Fresh (dotted line) synthetized iron oxide MNPs.

The size and morphology of the Fresh MNPs were evaluated by TEM, which is presented in Figure 3.5. The Fresh magnetite NPs were observed to be nearly spherical in shape and highly aggregated (as already mentionated). The particle size distribution histogram, shown in Figure 3.6 has been constructed from the image analysis of the Figure 3.5(a) using ImageJ software.[140] The mean particle size calculated is 9.81 nm with a standard deviation of 2.87 nm and a standard error of the mean as 36.1%. The particle size distribution observed from TEM is in the same range of crystallite size determined from the refinement of the X-ray diffraction. The differences may be assigned to huge difficulty in measuring the particles due to the high aggregation degree.

The lattice fringes of the produced MNPs can be seen in Figure 3.5b), which demonstrate that synthesized nanoparticles are crystalline.

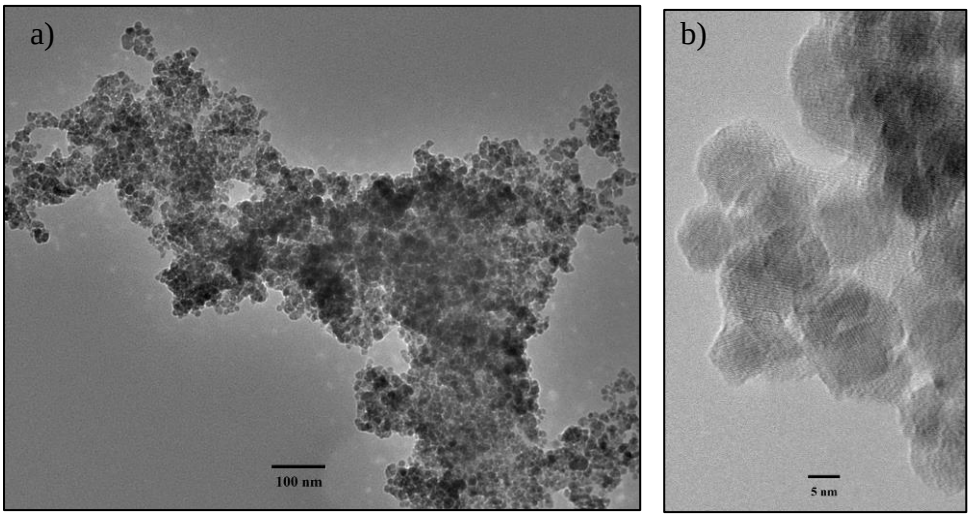

Figure 3.5 TEM images of fresh MNPs synthetized Fresh MNPs: a) overall view demonstrating the huge aggregation; b) the lattice fringes of the planes of the iron crystal structure.

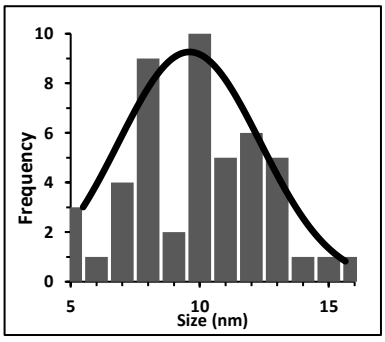

Figure 3.6 Size histogram showing the average diameter (9.81 nm) of the synthesized nanoparticles.

3.2 Linkage agents to enable the MNPs coating

Once we are dealing with very small particles, the high surface area makes them more susceptible to oxidation processes that can occur on their surface.[141] The coating of MNPs is a great solution to avoid oxidation. More, human body is composed by more than 70% of water, which means having a neutral pH. The produced MNPs are unstable in neutral pH (as it was observed in the Zeta Potential measurements, see Figure 3.17) and aggregates to be more stable, resulting in large agglomerates of NPs. Moreover, aggregated MNPs are not very effective in producing heating. So, to significantly improve the heating efficiency, disaggregation is need, because large hydrodynamic sizes slow down the Brownian

relaxation diminishing the heating efficiency. So, the particles must be disaggregated to achieve faster relaxations.[61]

The type of coating of the NPs is an important factor, because the MNPs can enter in the body by different ports, circulating through the lymphatic system and/or the bloodstream, either freely or after being phagocytosed.[68] So, it is important to have a stable coating, able to remain on the particles, even when they are exposed to interaction. The biocompatible coating proposed in this Thesis involves the biopolymer chitosan and to promote strong link of chitosan in to the iron oxide NPs it was used two linkages molecules: the dopamine and the caffeic acid.

3.2.1 Linking with Dopamine

Xu et al.[81] reported the use of dopamine, a natural molecule, as an attractive ligand to hydrophilic NPs of iron oxide, due to the strong interaction between vicinal diol groups to the iron oxide surface. In addition to be a stable to anchor, dopamine can work as a bridging ligand bonding other molecules through the amine groups.[81,127,142]

The FTIR spectra of dopamine (DOPA), iron oxide NPs functionalized with dopamine (F.DOPA) and MNPs are presented in Figure 3.7. Dopamine showed at 1616 cm^{-1}, 1497 cm^{-1}, 877 cm^{-1} (primary amine bending) and at 3336 cm^{-1} (stretching modes),[143] at 1471 cm^{-1} and at 3036 cm^{-1} (aromatic C=C symmetric stretching), at 598 cm^{-1} (C-C-C symmetric bending) and at 2953 cm^{-1} (C-H symmetric stretching).[144]

In the spectra of F.DOPA the characteristic peak of Fe-O at 533 cm^{-1} still present and the appearance of peaks at 1600 cm^{-1}, 1485 cm^{-1} and 872 cm^{-1} (primary amine bending) confirms the link between the MNPs and dopamine.[145] Further, the appearance peaks in F.DOPA spectra at 1398 cm^{-1} (hydrogen stretching vibration), at 2801 cm^{-1} (skeleton stretching vibration of benzene ring),[86] at 1031 cm^{-1} (stretching vibration of O–H), at 2847 cm^{-1} (stretching vibration of C–H), the broad band at 3300–3450 cm^{-1} (representing the stretching vibration of –OH),[110] at 693 cm^{-1} (C-C-C symmetric bending), at 1089 cm^{-1} (C-C-H symmetric bending)[144] supports even more that the conjugation of dopamine onto iron oxide was reached.

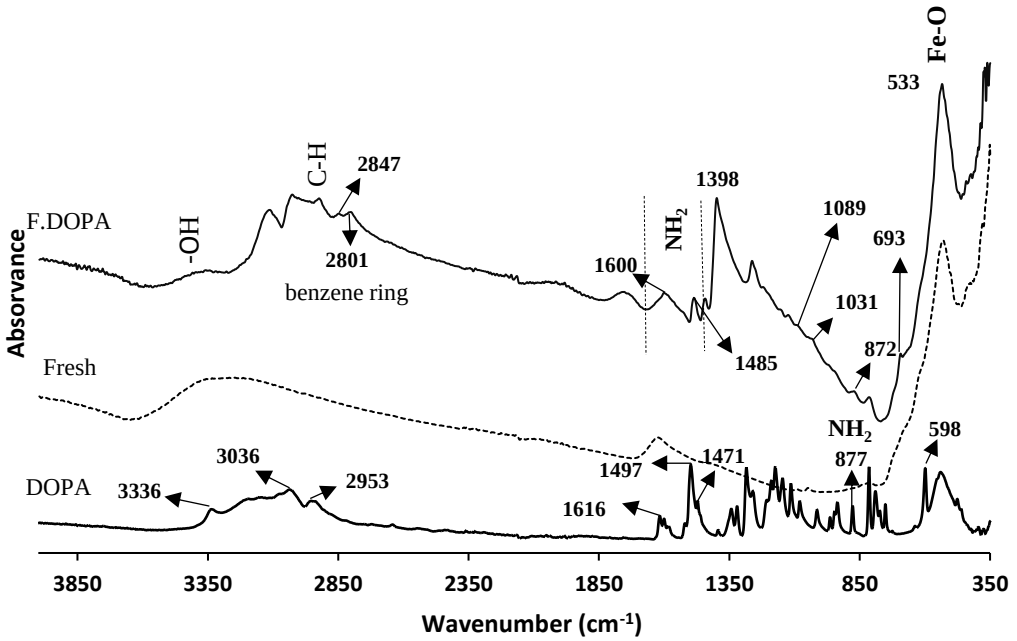

Figure 3.7 FTIR spectra of pristine Dopamine (DOPA), Fresh Fe_3O_4 and Fe_3O_4 conjugated with dopamine (F.DOPA).

3.2.2 Addition of Genipin

Genipin (GP), present in Figure 3.8, is a natural crosslinker with high biocompatibility and stability to heat, pH and light than the most used synthetic crosslinking agent glutaraldehyde.[60,146] Further, it was reported that GP might be about 5000–10.000 times less cytotoxic than glutaraldehyde.[125,147] Additionally, can naturally and effectively react with primary amino groups.[60] Furthermore, it was reported that the reaction of the GP with the amino groups of chitosan, make them insoluble to acidic medium.[147,148]

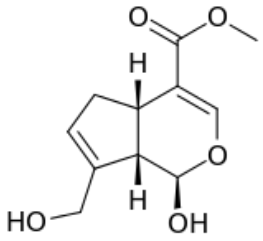

Figure 3.8 Chemical structure of genipin.

FTIR spectra of the tethering of GP into F.DOPA (F.DOPA.GP) is present in Figure 3.9.

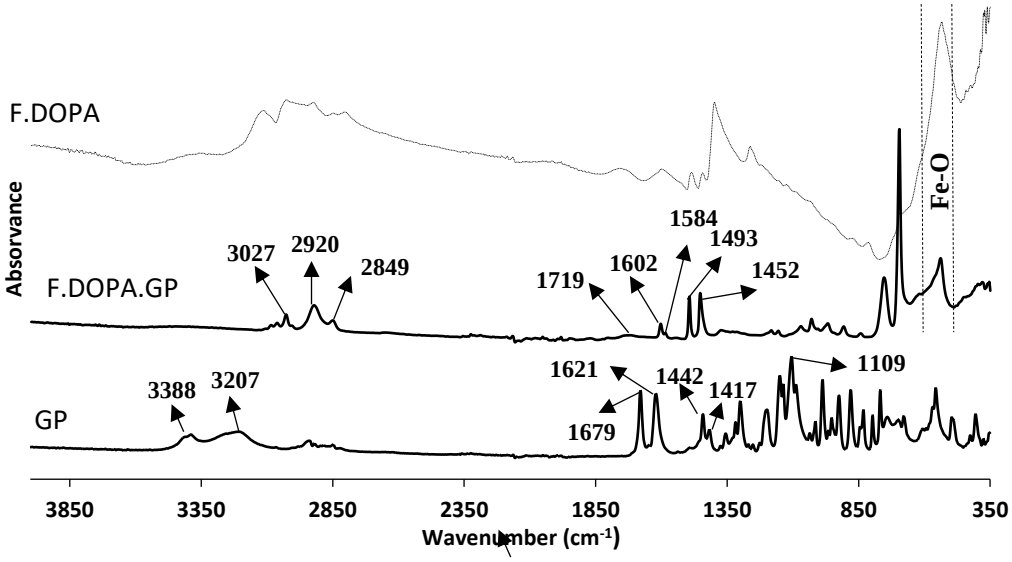

Figure 3.9 FTIR spectra of genipin (GP), F.DOPA and F.DOPA conjugated with GP (F.DOPA.GP).

The assignments of the bands in the GP spectra presented in Figure 3.9 were as follows: at 1679 cm^{-1} (C=O stretching vibration of the ester),[149–151] at 1109cm^{-1} (C-O-C stretch),[151] at 3388 cm^{-1} (associate O–H stretching vibration), at 3207 cm^{-1} (C=C–H stretching vibration)[149] and at 1621 cm^{-1} (C=C stretching vibration of the ring).[149,151] The band at 1417 cm^{-1} was assigned to a ring stretching mode in the GP molecule.[146]

When GP was bounded to the F.DOPA NPs, the peaks at 1679 cm^{-1}, the peaks at 1109 cm^{-1} and at 1621 cm^{-1} disappeared in cross-linked NPs of F.DOPA. The appearance of a weak absorption at 1584 cm^{-1} (C=C stretch of alkene) and at 1719 cm^{-1} (corresponding C=O stretch) revealed the ring-opening. The appearance of a peak at 1452 cm^{-1} (C=O stretch of carboxylic ion)[151] and the disappearance of the peak at 1442 cm^{-1} (stretching of methyl group of GP)[150] suggest that the ester groups were converted into carboxylic ions. A decrease in the characteristic peak derived from amine (-OH) stretch between 3500-3200 cm^{-1} [152] presents in GP FTIR spectra after crosslink into F.DOPA NPs was notice. More the aromatic peaks of dopamine are notice and shifts to lower values at 3027 and 2920 cm^{-1}.

3.2.3 Linking with Caffeic Acid

Caffeic acid (CA) is an organic compound classified as hydroxycinnamic acid[153] that have 14attracted attention in the last few years because of their biological properties as

antioxidant, immunomodulatory, anti-inflammatory, and anticarcinogenic activities.[85,154,155] Further, have a structural similarity to dopamine as it possible to see in Figure 3.10.

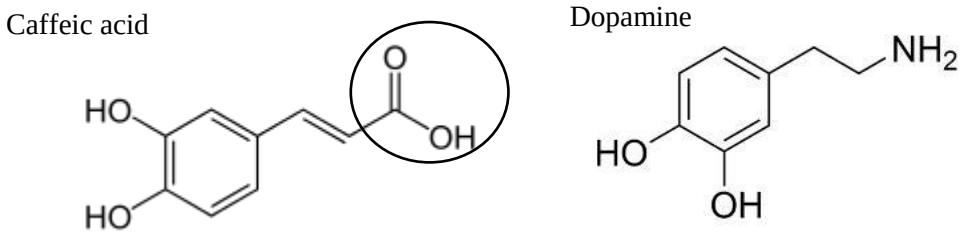

Figure 3.10 Chemical structure of caffeic acid and dopamine.

FTIR spectra of CA, iron oxide MNPs conjugated with CA (F.CA) and iron oxide MNPs are presented in Figure 3.11. Three characteristic peaks in CA spectrum are shown: at 1616 cm^{-1} (C=O stretching of free carboxylic acids), at 1598 cm^{-1} (asymmetric COO^- stretching) and at 1447 cm^{-1} (symmetric COO^- stretching). Further at 2983 cm^{-1} (asymmetric CH_2), at 2832 cm^{-1} (symmetric CH_2 stretching) and the band at 3400 – 3200 cm^{-1} (carboxylic acid -OH stretching).

The functionalization onto the iron oxide of CA was essentially made by the catechol group. The strong peak at 1598 cm^{-1} of pure CA, which points out the C=O vibration (symmetric stretching) from the COOH, remains but shifts to 1577 cm^{-1} and becomes weaker in the F.CA sample. A large and intense band between 3400-3200 cm^{-1} that could be assigned to the structural OH groups as well as to the traces of molecular water are present.[84,153,156] The peaks between 1200–1500 cm^{-1} and 800–850 cm^{-1} can be assigned to the presence of caffeic acid aromatic ring. The aromatic ring C=C stretching is within the 1450–1600 cm^{-1}; C-O/C-C stretching vibrations are within the 1200–1300 cm^{-1}.[126]

Additionally, it is possible to see the metal–oxygen band at 537 cm^{-1} corresponding to intrinsic stretching vibrations of the iron oxide. Thus, concluding that the functionalization was achieved.

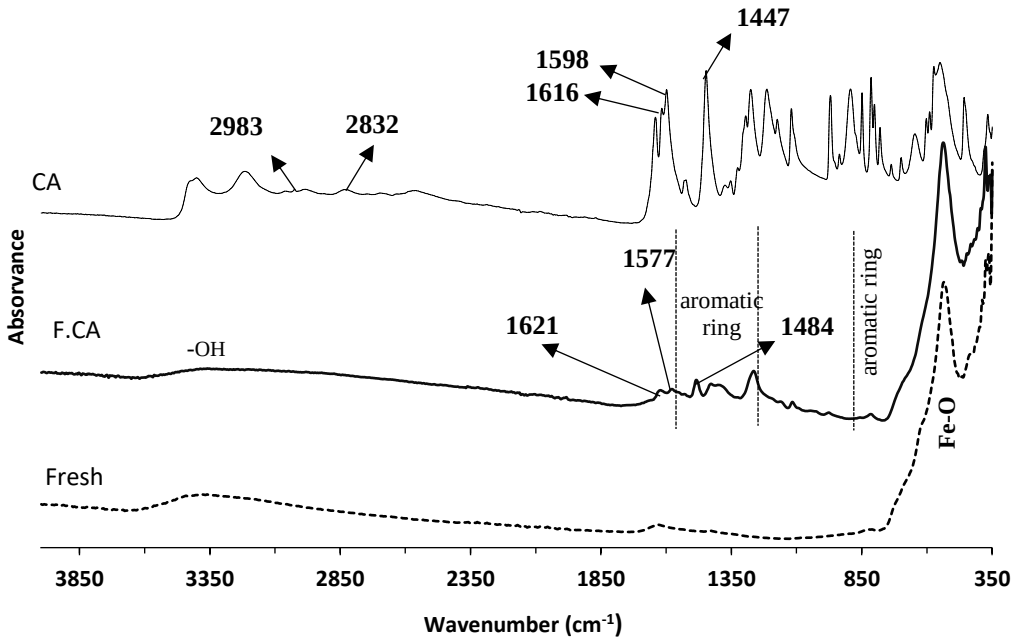

Figure 3.11 FTIR spectra of pure Caffeic acid CA, Fresh iron oxide MNPs and when conjugated with caffeic acid (F.CA).

3.2.4 Thermogravimetric analyses of the functionalized particles

TGA provides additional quantitative evidence of the coating of the MNPs surface.[18,73] By this technique it is possible to determine the thermal stability of the coated MNPs.[17,65,73]

In Figure 3.12 is possible to see the differences in thermal behaviour during the analysis. As expected, the MNPs were not degraded from room temperature until 400 ºC.[100] Only the organic part of the coating suffer degradation. Until 150 ºC, the weight losses occurred are attributed to the removal of physically and chemically adsorbed water.[17,71,84,153] Above this temperature the MNPs can lose the hydroxyl groups present at the surface and then organic groups start to be degraded.

The Old and Fresh MNPs have different behaviours as expected from the distinct degree of oxidation. The Old MNPs show about 19% of total weigh, corresponding to near only 4.5% of water loss and about 15% of weight loss between 180ºC and 260ºC assigned to release of hydroxyl groups from the surface of the particles. The total weight loss observed in Fresh NPs were only 3.5%, where 2.2% corresponds to water loss up to 150 ºC. This results are in agreement with others of literature.[17,73] The 0.01% of loss above 400ºC observed in Fresh MNPs may be due to some oxidation in the surface of the MNPs of magnetite that occurs in

the presence of air atmosphere (it is possible to see some endothermic peak from 400 ºC to 600 ºC). Further, comparing the Old and Fresh MNPs, the Old MNPs do not have endothermic process at high temperatures, probably because the Old MNPs surface was already oxidized (passivated). So, it is possible to conclude that in Fresh NPs the amount of magnetite is greater than in Old NPs.

Regarding to the functionalized NPs, namely the F.CA, it is possible to see that caffeic acid starts to decompose at 200 ºC.[84,153] There are two exothermic peaks, a great one about 200 ºC and at 300 ºC.[84,153] It is possible to observe a small endothermic peak about 400 ºC. The greater loss of organic mass observed in Old MNPs should be the result of high yield of the coating reaction with consequent better coverage of the NPs surface.

The decomposition of dopamine have two major stages, one at 200 ºC, which is due to the decomposition of ethylamine arm NH_2[30] and another at 500 ºC concerning the decomposition of the aromatic ring. Relatively to the F.DOPA NPs, it is possible to see that the differences between Old and Fresh NPs spectra are bigger than in the case of caffeic acid. The Fresh NPs after reacting with dopamine seem to have a TGA curve very similar to the one non-oxidized pure particles. The Old F.DOPA seems to have a higher content of DOPA ligand that the Fresh F.DOPA. The first weight loss occurs at 40 ºC (which corresponds to water loss) and then, in the Old NPs we have a mass loss at about 200ºC, which is the same range of temperature where the dopamine stars to decompose. The release of hydroxyl groups at the surface at the iron oxide NPs also happen in this range of temperatures. Observing the peaks, we can assume that the weigh losses are not only caused by dopamine decomposition but also results from the decomposition of oxidation moieties losses from the iron oxide, once has the same behaviour of Old MNPs.

More, the incorporation of the respective DOPA functionalization did not seem to avoid the oxidation of the particles or they were not fully covered by DOPA. The continuous variations in decomposition on the functionalized samples indicate that the bonds between the organic material (caffeic acid and dopamine) and the core of iron oxide are of a chemical nature, stronger than physical bonds. Therefore, this functionalization is stable and adequate to biomedical applications.[30]

Table 3.3 shows the percentages of mass losses observed in the TGA analyses for the Fresh and Old iron oxide and when linked with CA and DOPA

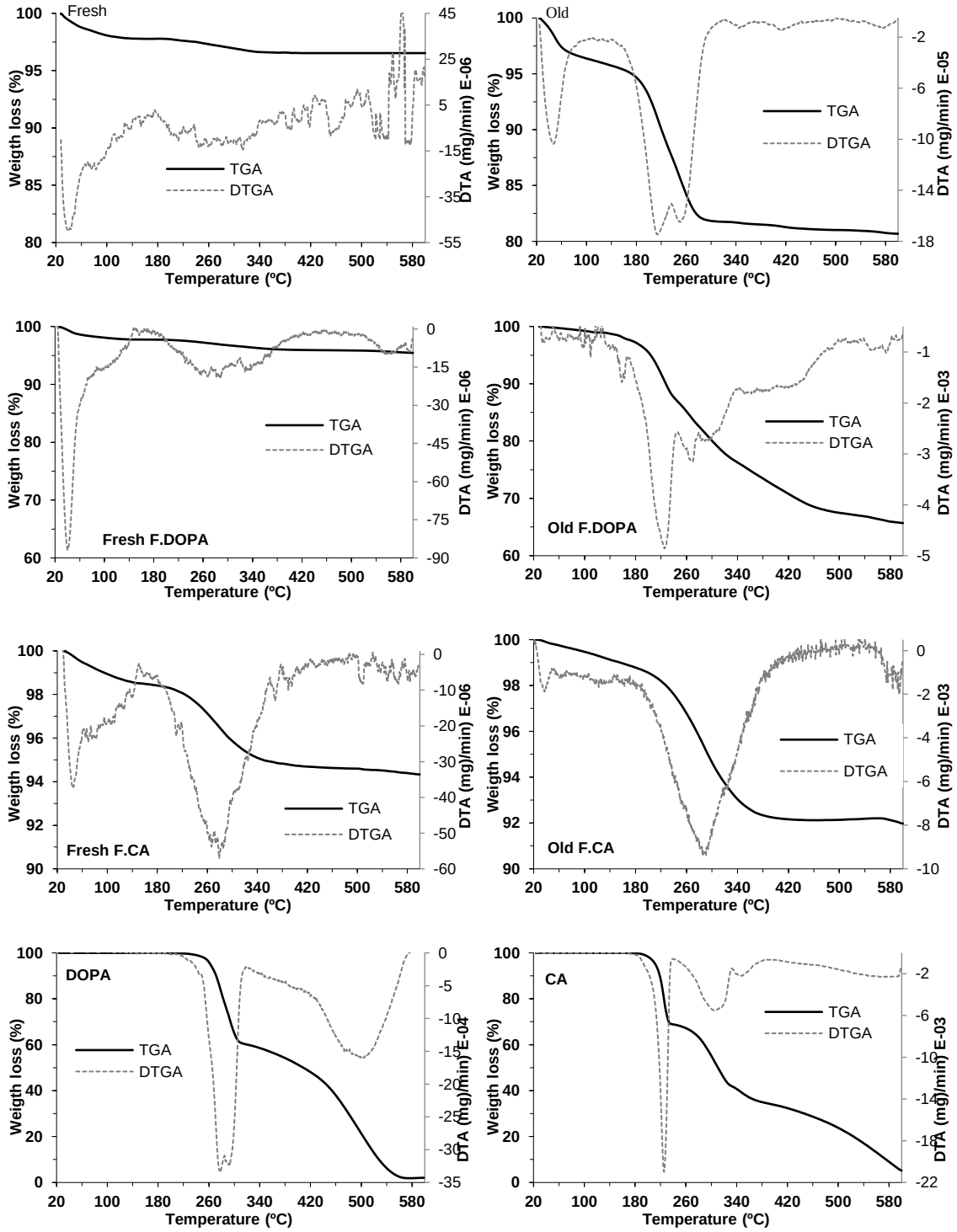

Figure 3.12 TGA analysis of a dried samples of Fresh and Old iron oxide; and when both (Fresh and OLD MNPs) conjugated with dopamine (DOPA) and caffeic acid (CA); and the pure DOPA and pure CA.

Table 3.3 Summary of the percentage of mass losses during the TGA analysis observed for the Fresh and Old NPs and when conjugated with DOPA and CA

Temperature (ºC)	**FRESH MNPS % weigh loss**			**OLD MNPS % weigh loss**		
	F	**F.DOPA**	**F.CA**	**F**	**F.DOPA**	**F.CA**
> 150	2.21	2.25	1.48	4.43	1.46	0.95
150-400	1.25	1.77	3.77	14.14	26.39	6.83
< 400	0.01	0.54	0.401	0.75	6.44	0.24
Total	3.47	4.56	5.67	19.32	34.29	8.02

3.2.5 Chitosan coating

The MNPs were coated with chitosan polymer aiming to protect the iron oxide core and maximizing its stability. The bonding between chitosan and the respective binders were confirmed by FTIR measurements.

3.2.5.1 Coating F.DOPA.GP MNPs with chitosan

The coat of chitosan to the MNPs conjugated with dopamine and tethering with genipin was confirmed by FTIR. The Figure 3.13 shows the FTIR spectra of the chitosan (CS) and MNPs of F.DOPA.GP and coated with CS (F.DOPA.GP.CS).

In the CS spectra were found bands at 1645, 1574 and 1316 cm^{-1} which were assigned to the (C=O stretching (amide I)),[101,157] (N-H bending (amide II))[101,147,157] and (C-N stretching (amide II)) of the residual N-acetyl groups, respectively.[101,157] The peaks at 1376 cm^{-1} were attributed to (C-O-H stretching) of a primary alcoholic group in chitosan. The absorption bands between 1000-1100 cm^{-1} were described to (C-O) and (C-N) stretching vibrations, and (C-C-N bending vibrations). The broad bands between 3000 - 3600 cm^{-1} were related to the hydroxyl groups mainly from water which probably overlaps the amine stretching vibrations (N-H) in the same region.[147,150,157] Significant absorption peaks at 895 and 1150 cm^{-1} appears, which corresponds to the C-O linkage of saccharide structure of glucosamine ring. One of the most important changes is evident in the reduction of the carbonyl group of the GP at 1719 cm^{-1}, which reacts with the primary amine in chitosan to form an amide, is

indicated by the growth of the absorption band at 1600 cm^{-1}. [147,158] The increase observed in the peaks at 1377 cm^{-1} (C-N stretching vibrations),[147] the appearance of characteristic peaks of (NH_2 asymmetric stretching) at 3407 cm^{-1} [158] prove that chitosan has been reacted with the ligands at the NPs surface

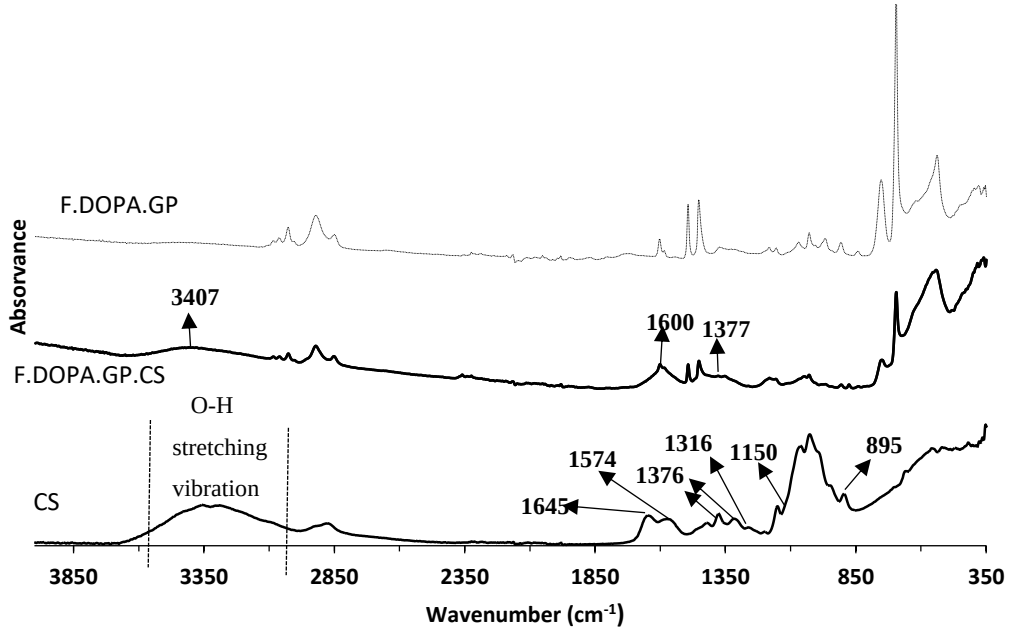

Figure 3.13 FTIR spectra of chitosan (CS), F.DOPA.GP and F.DOPA.GP coated with CS.

3.2.5.2 Coating of the F.CA MNPs with chitosan

The coat with CS onto functionalized NPS with caffeic acid (F.CA) was tested by two different routes: using EDAC chemistry through the creation of amide bonds between a carboxylic acid group in CA and a primary amine group in CS and through (CAN). The successful conjugation of CS onto the F.CA NPs was confirmed by FTIR. The Figure 3.14 shows the FT-IR spectra of raw CS alone, F.CA and after the coating with CS using the EDAC and CAN procedures to get the coating. It is possible to see that typical bonds of chitosan are present in both spectra. The C=O peak at 1577 cm^{-1} present in F.CA spectrum disappeared in the both spectra after the coat with CS (via CAN and via EDAC), confirming the successful coupling between the carboxylate groups of CA and the amino groups of CS.[156] No band appeared at 1730 cm^{-1} in both spectra (as it evidenced by the circle), indicating that no ester bond formed between hydroxyl groups of chitosan and carboxyl groups of phenolic acids.[101]The broad absorption peaks in the range of 3000–3450 cm^{-1}

observed in CAN and EDC spectra are due to the chitosan OH groups stretching overlapping the N-H stretching.[40,85] The bands related to the C-O-C bridge are located at 1152/1091cm^{-1} (anti-symmetric stretching of C-O-C bridge). At 1028 cm^{-1} (skeleton vibration involving the C-O-C stretching bands)[85,125] and at 823/814 cm^{-1} (C-O-C stretching of the glycosidic linkage)[85] of CAN and EDAC respectively. Vibration modes at 1419/1429 and at 1316/1321 cm^{-1} assigned to O–H (originating from CS)[157] are presented in CAN/EDAC. The absorption decrease associated with protonated glucosamine residues of chitosan at 1326 and 1427 cm^{-1} indicated a covalent linkage between phenolic acids and the amino groups of chitosan.[101] The band at ~1060 cm^{-1} is attributed to the C-N stretching vibration mode. Additionally, the second band of the amide II (usually found around 1574 cm^{-1}) disappeared and a new band at ~1550/1541 cm^{-1} appeared which corresponds to the N-O asymmetric stretching vibration mode, confirming the ionic bond between chitosan and CA[85] in the spectra of CAN and EDAC respectively. The band at 528 cm^{-1} in CAN spectrum and at 536 cm^{-1} in EDAC spectruma is attributed to Fe-O stretching vibration mode related to the presence of iron oxide.

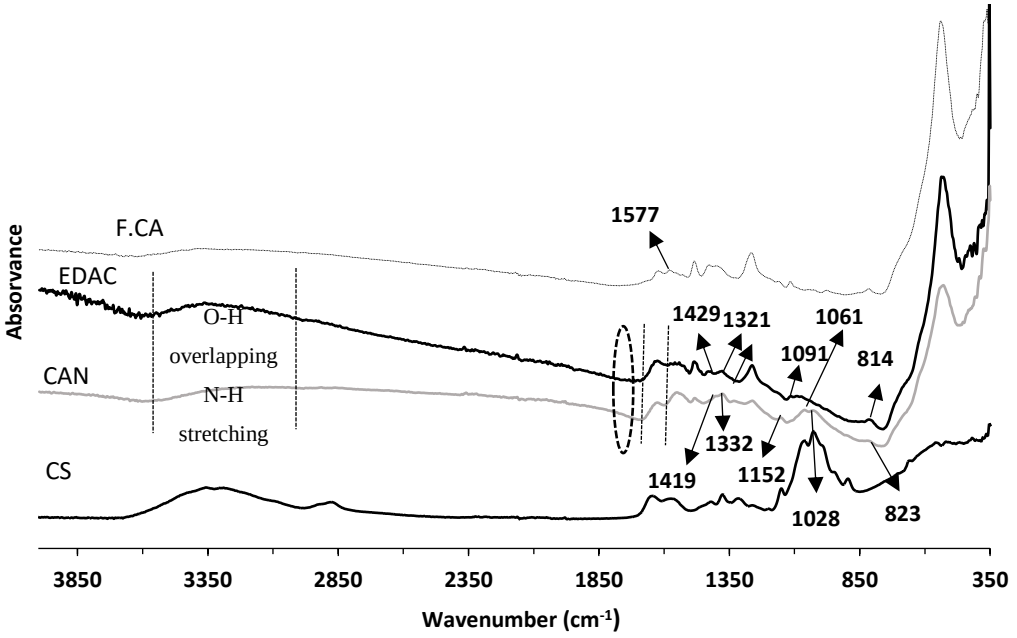

Figure 3.14 FTIR spectra of the MNPs functionalized with CA, and coated with chitosan per two different methods: CAN and EDAC.

3.2.6 Thermogravimetric Analyses of chitosan coated MNPs

Figure 3.15 show the results of the TGA analyses for the samples coated with chitosan and the chitosan used for the coating.

TGA of pure CS exhibited two distinct stages. The first weight loss of ~13% observed up to 150 ºC was due to loss of water from the polymer composites. The second one, between 150 ºC and 400 ºC is ascribed to a complex process including dehydration of the sugar rings, depolymerization and decomposition of the acetylated and deacetylated units of the polymer. This complex process represented about 47%. As compared to CS, CAN and EDAC have two exothermic peaks in the same temperature regions. The first loss, up to 150ºC correspond to the water loss. The second one, is due to the degradations of the grafted products (CA and CS). In addition, differential thermogravimetry (DTGA) curves showed that the temperature for the rapidest weight losses of chitosan appeared at 297 ºC in CAN at 257 ºC and in EDAC at 267.3 ºC. This indicates that the thermal stability of CS was reduced after coating. These results are consistent with others studies. In general, the introduction of functional groups can result in decreasing of thermal stability.[101] The thermal stability of EDAC was higher than CAN. This difference may also be due to a higher amount of coating present in the EDAC sample (11.6%) than in the CAN sample (7.3%).

Table 3.4 shows all the percentages of weight losses observed in TGA analysis of the samples up to the coating with chitosan.

Table 3.4 Summary of TGA percentage of weight losses of all samples.

Temperature (ºC)	**% Weight losses**						
	F	F.DOPA	F.CA	CAN	EDAC	F.DOPA.GP.CS	CS
> 150	22.1	2.25	1.4	1.89	1.93	0.00	12.58
150-400	1.25	1.77	3.77	5.21	9.58	5.93	46.96
< 400	0.01	0.54	0.41	0.2	0.07	10.75	28.17
Total	3.47	4.56	5.67	7.30	11.58	16.68	87.71

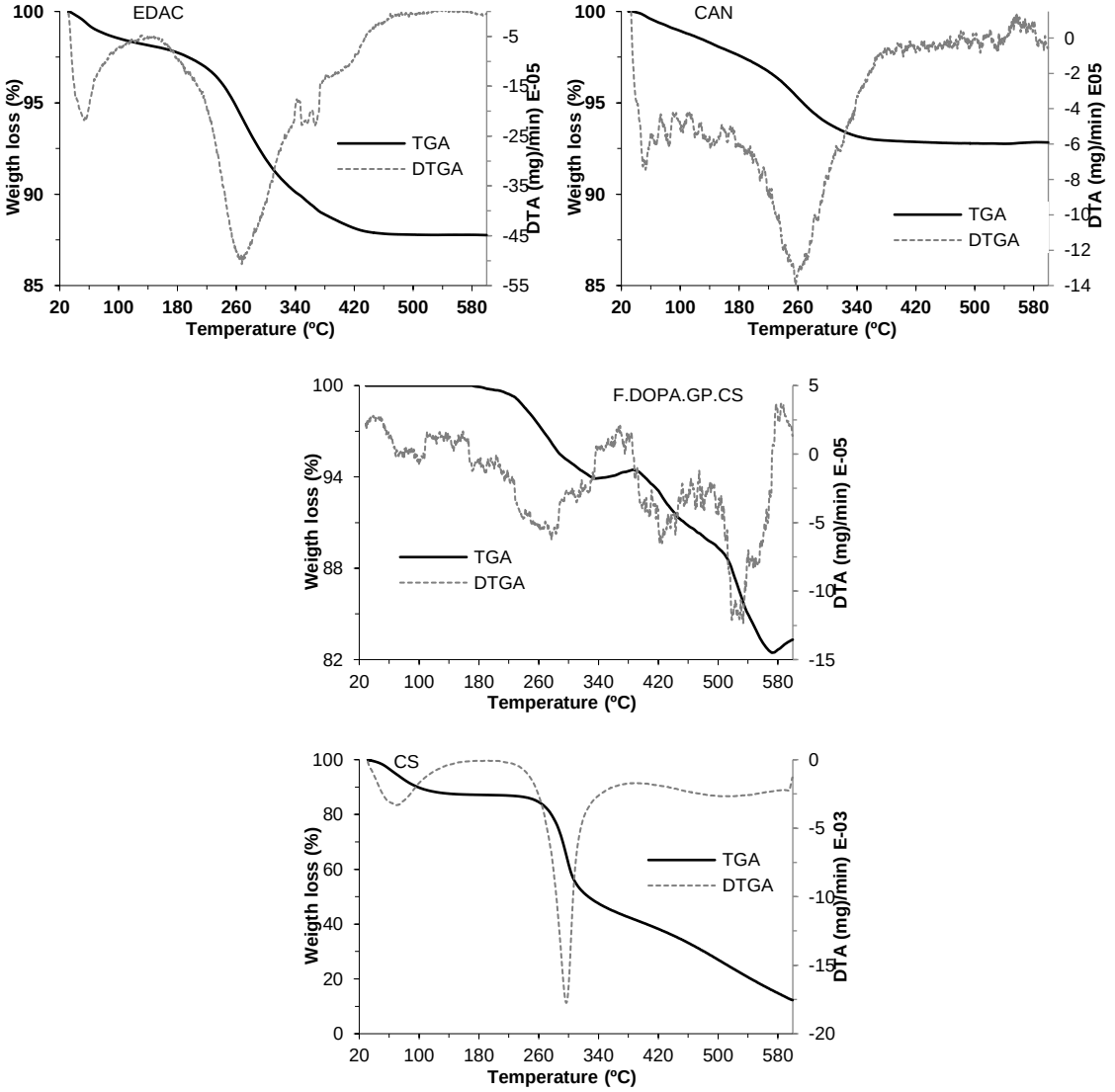

Figure 3.15 TGA analysis of the coated with chitosan of the Fresh MNPs conjugated with caffeic acid using cerium ammonium nitrate (IV) (CAN) and using EDAC chemistry (EDAC); and the MNPs coated with chitosan conjugated with dopamine and genipin (F.DOPA.GP.CS) and the raw chitosan (CS).

TEM images of the coating with chitosan is shown in Figure 3.16. All the samples maintained their original type spherical shape and the coated provide by the CS is very well observed (evidenced by arrows). There is a huge difference in aggregation in uncoated and coated MNPs, which decreases immensely after the functionalization with ligands and with chitosan. In the case of the NPs functionalized with dopamine and genipin before the coating with chitosan, the level in aggregation seriously decrease when compared with the initial NPs. Further, it appears to have a more proportional coating along the NPs with this method than EDAC or CAN. Still, by all methods the coating with chitosan was achieved. However,

some optimization is need in the case of EDAC and CAN. There are some NPs that seem to have less or no coating at all. It is possible to see that the average particle size after the coat is much higher than initial NPs.

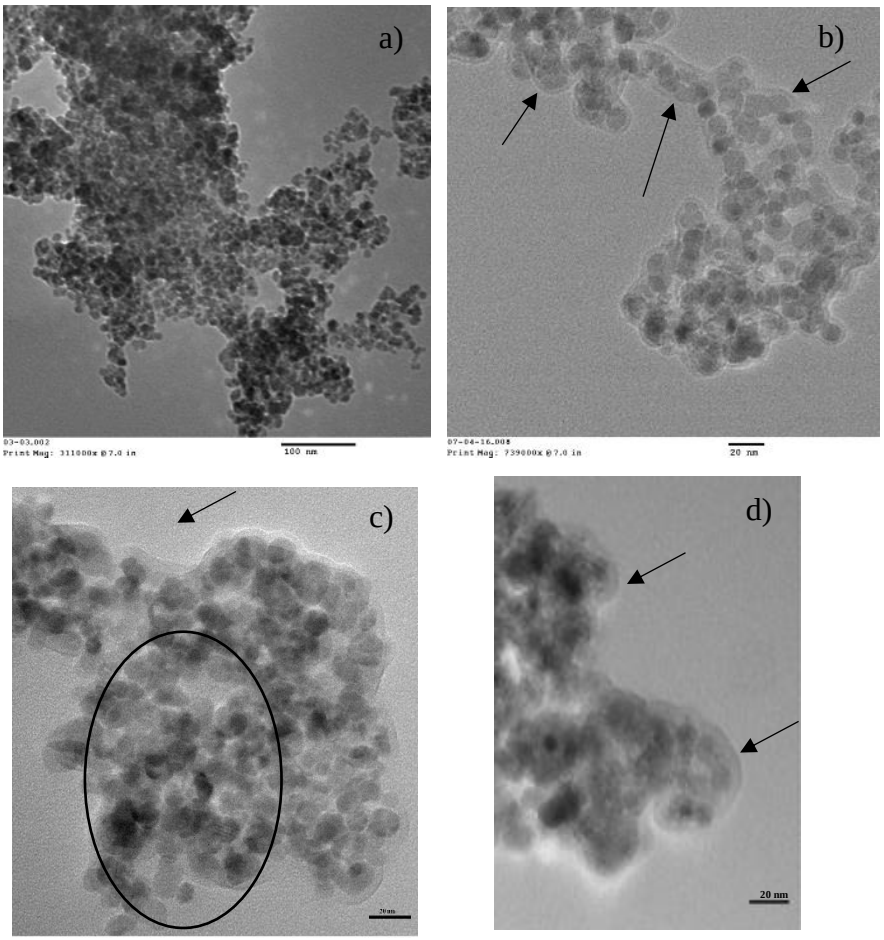

Figure 3.16 TEM images of: (a) uncoated MNPs; (b) MNPs functionalized with dopamine and with genipin and coated with chitosan (F.DOPA.GP.CS); (c) MNPs functionalized with caffeic acid and coated with chitosan via EDAC; d) MNPs functionalized with caffeic acid and coated with chitosan via CAN. The arrows evidence the coat of chitosan. The circle evidence the absence of the coat.

3.2.7 Zeta Potential and Hydrodynamic Diameter of funcionalized and coated MNPs

The Zeta Potential values and hydrodynamic diameters of some of the NPs synthesized with respect to pH 2 to 12 are shown in Figure 3.17 and Table 3.5, respectively.

As it possible to see in Figure 3.17, the Zeta Potential of the NPs ranged from -40 eV to 40 eV. In physiological pH, the zeta potential was about -17 mV, -30 mV and 33 mV in Fresh MNPs, F.CA and F.DOPA respectively. These results show the increase in stability after the conjugation.

The isoelectric point (PI) for MNPs was found to be around 3.5 and possess negative charge at physiological pH. These observations are in agreement with other literature as (17). When dopamine was added to the particles, this value shift to 9.3. The reactions of the MNPs with CA, results in a shift of the P.I. value to 4.5. Through observation on these results of the Zeta Potential of F.DOPA and F.CA samples are more positive in the range of pH 2–4.3 and more negative after pH 10, in comparison to the Fresh un-conjugated MNP. This indicates that the positive charges on the coated NPs increase with a decrease in pH and the negative charges on the coated NPs increase with increasing in pH. Proving by this way that the particles were functionalized. These results indicate that the functionalization with DOPA and CA can provide a steric barrier between the MNPs particles when pH value of the medium is acidic or basic, thus decreasing the agglomeration of the MNPs. The coverage provided by the functionalization on the unconjugated MNPs surface can stabilize the particles in water media. Although, the MNPs conjugated with dopamine shows a better colloidal stability in acid media than bare Fe_3O_4 and when conjugated with CA. The fact that F.DOPA is much more positive in the range of pH 2 up to pH 10 than Fresh MNPs and F.CA allow crosslinking with GP in more individualized was because of a greater steric barrier. But, when the GP is added, their stability decrease. This proves that the crosslinking occurred because adding the GP to the F.DOPA the results where similar to the F.CA sample. This is because both have free OH^- in their structure. However, in the F.DOPA.GP analysis the stability is lower than in the F.CA sample in acid and neutral pH, being identical in high pH. This is probably because the F.DOPA.GP do not have much charge, being instable and allowing aggregation of the MNPs.

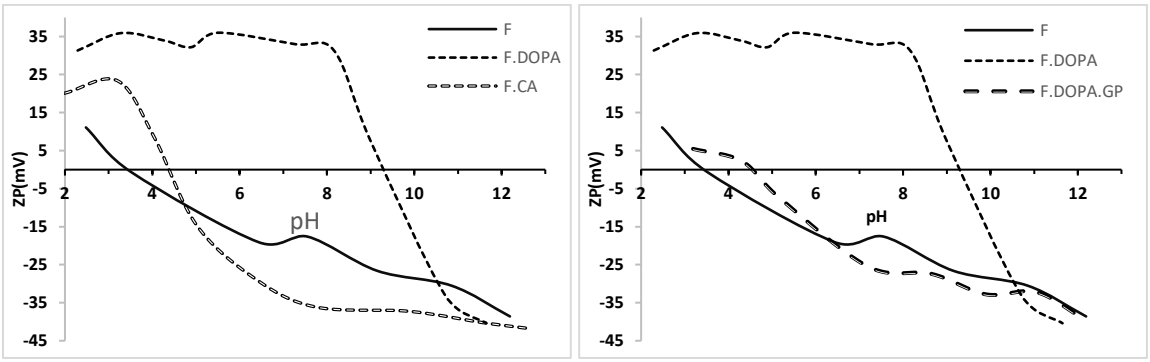

Figure 3.17 Zeta Potential of the initial MNPs (F) and when functionalized with dopamine (F.DOPA) and crosslinked with Genipin (F.DOPA.GP) and with caffeic acid (F.CA).

The hydrodynamic sizes of Fresh MNPs and functionalized NPs were measured using dynamic light scattering (DLS). Table 3.5 shows the hydrodynamic diameter distribution of bare and capped MNPs in filtered water. The density of the polymeric structure can affect the properties of the composites NPs.[100] The particle size measurements do not match with the crystallite size calculated from XRD pattern, confirming the aggregation in the MNPs and the instability of the fluid.[133] Especially when close to their respective PI values, where the MNPs showed highest hydrodynamic diameters due to highest degree of agglomeration. The uncoated MNPs have larger size due to higher degree of agglomeration and consequently show lager hydrodynamic diameter than the coated ones. However, the same way as happened with the analyses of TEM images. The mean diameter of the MNPs coated with chitosan increase, proving that the coating with chitosan was achieved.

Polydispersity degree indices (PDIs) lower than 0.25 shows a monomodal distribution.[71] The stirring the mixtures before the analysis does not influence size of MNPs, since the MNPs settle during the analysis whatever the time during which the solution was stirred.

Although knowing that the hydrodynamic size obtained from DLS were not correct, it is possible to see a decrease on the diameter after reaction of the MNPs with DOPA. This decrease did not happen with CA, thereby highlighting that dopamine is a better option concerning to the dispersion of particles, leading to high colloidal stability. After the addition of GP to the F.DOPA NPs, a huge increase in the diameter was noticed by the DLS analysis. This is probably due to polymerization of GP. However, the addition of GP particles did not contribute to the increase in the colloidal stability. Moreover, the colloidal stability at acidic pH decreases to levels similar to unconjugated NPs as it is possible to see in Figure 3.17. The polydispersity (PDI) is a measure of the degree of non-uniformity, that is influenced by

the size, charge, magnetic field distribution, pH and coating.[9] A value between 0.1 and 0.4 is indicative of an intermediate, moderately polydisperse distribution type.[159]

Table 3.5 Hydrodynamic diameter of the iron oxide MNPs and with some of MPS with the ligand and the coat of chitosan. Z- represents the average size; Std - represent the standard deviation; d – represents the diameter in nm.

AMOSTRA	pH	Z	stdv	Pdi	stdv	Number Mean		Intensity Mean		Volume Mean	
						d	std	d	std	d	std
Fresh	6.22	345	1,127	0,47	0,067	137	7,1	467	93,88	665,2	210,4
F.DOPA	4.99	146.8	0.4619	0.215	0.015	72.71	8.655	225,9	45.5	248.8	97.39
F.DOPA.GP	5.90	346.7	25.1	0.243	0.011	265.9	21.21	354,3	29.3	385.2	42.57
F.DOPA.GP.CS	5.78	433.9	2.219	0.465	0.028	146.0	22.04	404.1	43.26	469.3	106.2
Fresh	6.22	345	1,127	0,47	0,067	137	7,1	467	93,88	665,2	210,4
F.CA	5.56	151.6	1.097	0.194	0.007	84.4	1.141	235,8	6.976	292.2	22.9
EDAC	5.62	401.5	5.009	0.39	0.016	158.6	9.536	566.4	47,04	835.8	99.67

It is possible to see that at about neutral pH, the functionalization decrease the hydrodynamic diameter both for NPs of F.DOPA and F.CA. Observing the results of intensity mean of before and after the add of the functionalization agents, is clear that the larger particles have decreased and were similar in both of them. This proves that the functionalization occurred as well as steric barrier that was provided.

The addition of the GP as tethering agent in the F.DOPA NPS resulted in an increase of Z-average diameter of the NPs to values similar to the iron oxide MNPs. But, a deeper look to the number mean, intensity mean as well volume mean, is observed that these do not increase to similar values of the iron oxide MNPs. This strength the steric barrier caused by the adding of the dopamine to the iron oxide. As genipin can easily bond amine groups of DOPA, and eventually reacted with other GP molecules[148] this results in a considerable increase of the hydrodynamic diameter.

The addition of CS to the functionalized NPs resulted in an increase of the hydrodynamic diameter, (more notice in the F.CA NPs) which confirms the coverage of the particles with chitosan, which is a biopolymer with a significant long chain.

3.2.8 Magnetic Characterization

The curves resulting from the study of the magnetization as a function of temperature (ZFC and FC) and of the magnetization as a function of the magnetic field for the iron oxide MNPs are shown in Figures 3.18 (Fresh and Old) and 3.19 (F.CA; F.DOPA; CAN; EDAC; and F.DOPA.GP.CS). The observation of these curves allows verifying a clear superparamagnetic behaviour of the MNPs at room temperature.

In general, the magnetic behaviours of the different samples are similar as well as the saturation and coercivity magnetization values. All samples exhibit ferrimagnetic behaviour as expected for magnetite type samples, displaying a high slope at low fields and saturating for external fields above 1 T. The coercivity and the remanent magnetization are very small. The analysis of the ZFC curves in Figures 3.18 and 3.19 shows a continuous increase up to 250 K indicating that the Fresh MNPs blocking temperature is above this temperature. This is consistent with the size of the magnetic nanoparticles (around 14.7 nm). The amount of iron oxide in composite particles was obtained from the corresponding saturated magnetic moment at 250 K, assuming the saturation magnetization obtained from the non-functionalized sample. The concentration of the iron oxide in the dispersions was obtained assuming that the density of the particle dispersion was close to one (density of water).

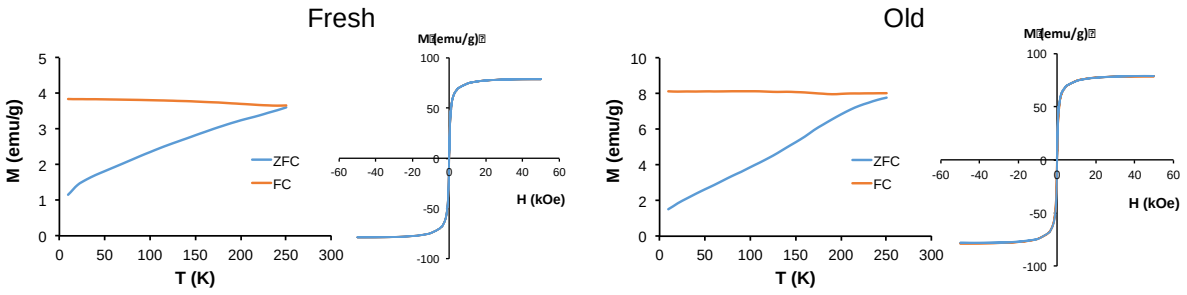

Figure 3.18 Magnetization curves as a function of temperature (up to 250 K) measured at 50 Oe, and magnetization curves as a function of the applied field of the iron oxide MNPs (Fresh and Old NPs).

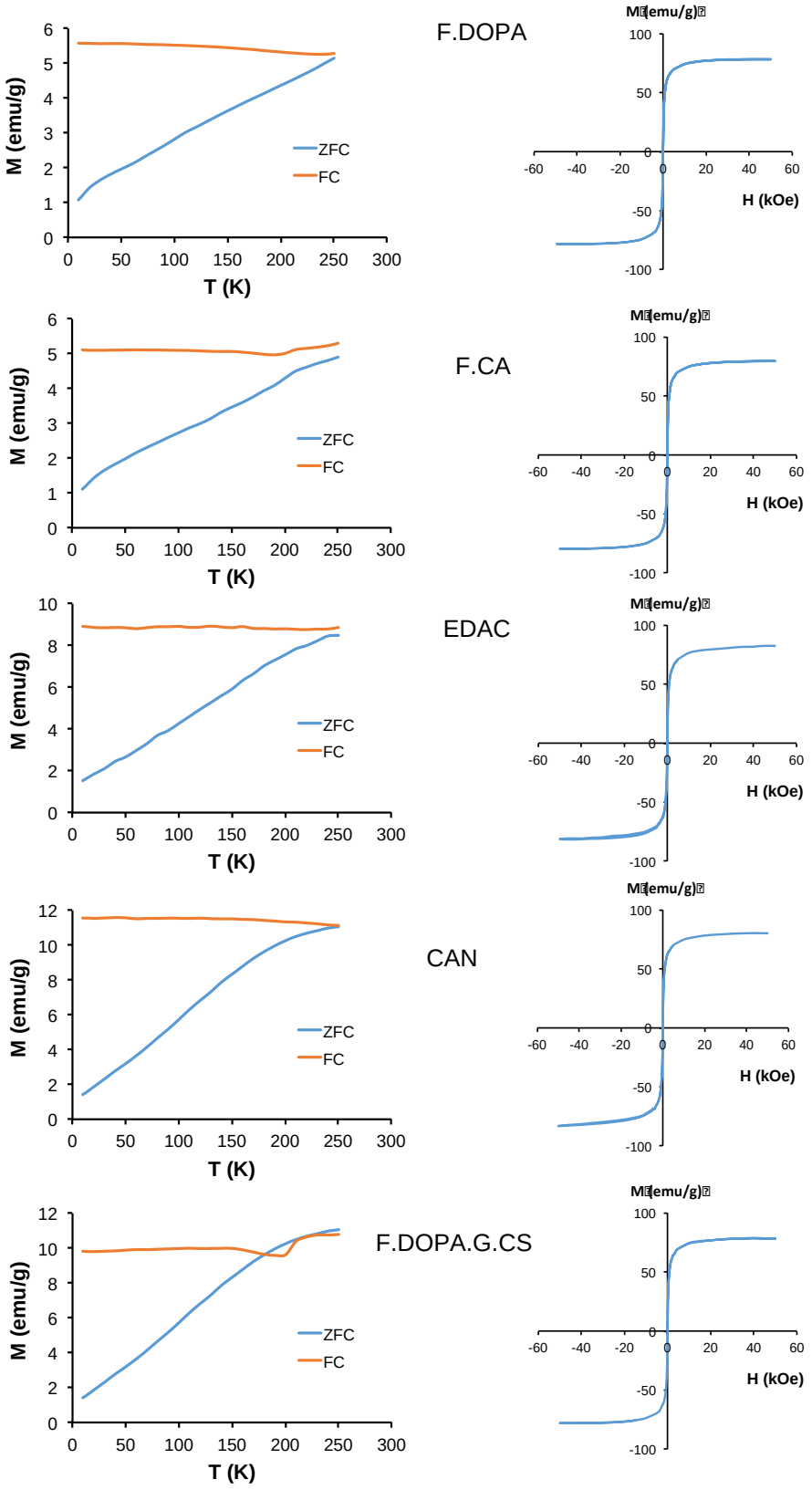

Figure 3.19 Magnetization curves as a function of temperature (0-250 K) measured at 50 Oe, and as a function of the applied field of the F.DOPA, F.DOPA.GP.CS, F.CA, EDAC, CAN.

The comparison of the magnetization curves as a function of the temperature in Figure 3.18 allows to verify that the ZFC and the FC curves in the Old NPs do not touch at high temperatures, providing an evidence of the partial oxidation of the iron. The same evidence was also verified when caffeic acid was used. In Figure 3.19, it is observed peaks in the ZFC curve near 200 ºC, assigned to oxidized magnetite.
The ZFC and FC curves of F.DOPA close at 250 °C, which indicates that these MNPs are the best dispersed, in agree with the Zeta Potential results.

3.2.9 Magnetic hyperthermia measurement

The study of the ability to release energy by the particles when subjected to an alternating magnetic field was performed for some sample previously mentioned. As explained above the results of these measurements give rise to a temperature vs time plot which provides the parameters required for determination of specific loss power (SLP) (Eq. 3.2). In this work and in order to determine this value with greater accuracy, the determination of the SLP values were determined by the following equation:

$$slope = \frac{\Delta T}{\Delta t}$$

$$SLP = slope \times \frac{(m_{glass} \times c_{glass} + 0.3 \times m_{water} \times c_{water})}{m_{NPs}} \qquad \text{(Eq. 3.2)}$$

Where ΔT is the variation of temperature, Δt is the time variation (in *s*), m_{NPs} is the mass of the sample (in g), m_{glass} and m_{water} are the mass of the glass (the quantity that was in contact with the sample ≈ 80% of the mass of the botlle) and the mass of water (in g), c_{glass} and c_{water} are the heat capacity of glass (0.2 cal g^{-1} $^{\circ}C^{-1}$) and the water (1.0 cal g^{-1} $^{\circ}C^{-1}$), respectively. The sum of the product of m_{glass} and c_{glass} with m_{water} and c_{water} correspond to the value of heat specific capacity, c (in cal ºC). 0.3 represents a factor related to heating absorbed by the glass during the measurement.
In the Figure 3.20 is found the assays performed on distilled water for the synthesized samples. In general, experimental values exhibit a progressive increase in temperature at the time of the stipulated period (160 s). In order to be able to correctly compare the results obtained with the different samples, the SLP values were calculated by equation 3.2. The

values obtained are summarized in Table 3.6. As we were measuring composite nanoparticles, and the concentration of magnetic nanoparticles was not completely known, the mass values were corrected assuming the magnetization of saturation of the pure MNPs. The values obtained for the SPL varied between 33 (in the F.DOPA.GP.CS) to near 55 W/g. The value in the obtained with the F.DOPA.GP.CS NPs relatively low in comparison with the others NPs could be the result of the some polymerization of the biopolymer CS and GP that occurs and trapped f NPs, diminishing their Brownian losses. and These results are quite promising as the coating conditions are not yet optimized.

The comparison of the SLP values obtained with other published values is difficult, since, the conditions of measurements strongly influence the results, and the authors do not always specify the measurement conditions in detail. On the other hand, factors such as: the applied magnetic field (coil used, frequency and current intensity); the magnetic properties of NPs (eg, saturation magnetization); the physical properties of NPs (in particular their size and dispersion), among other factors, also influence the determined values.

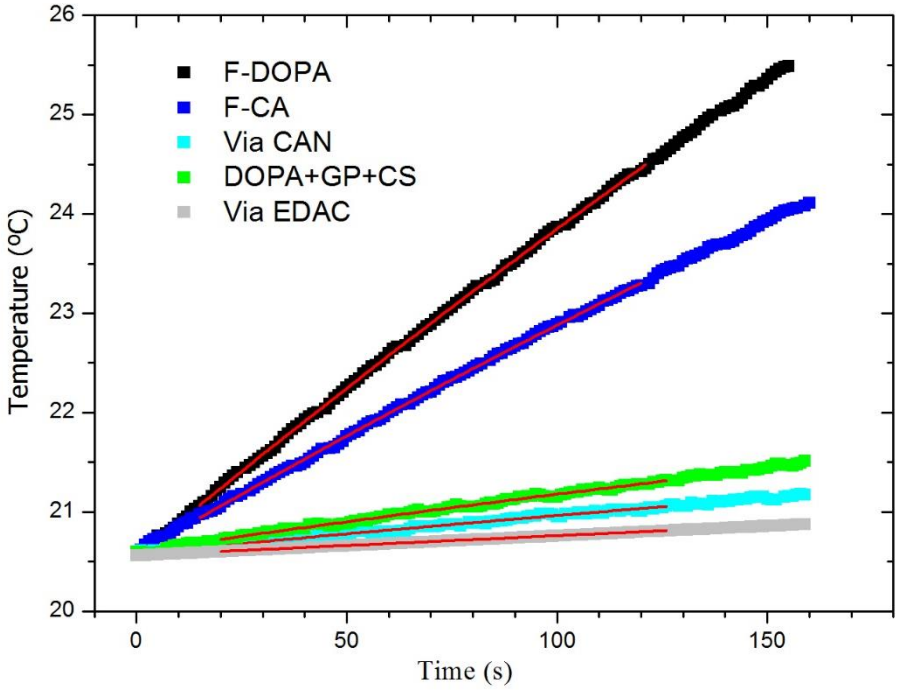

Figure 3.20 Temperature variation as a function of time for samples synthesized in distilled water when subjected to an alternating magnetic field.

Table 3.6 Values of the specific absorption rate of the synthesized samples, based on the results obtained. It is assumed that the mass of the dispersion is equal to the volume of water. c_{water}=4.185 (J / g K) and c_{glass}=0.2 (J / g K).

Sample	**slope**	**m_{glass} (g)**	**$m_{dispersion}$ (g)**	**c_{NPs} (g/ml)**	**m_{NPs} (g)**	**SLP (W/g)**
F.DOPA	0.03492	4.4331	2.941	2.76E-03	8.12E-03	54.1
F.CA	0.02444	4.4694	2.8981	2.02E-03	5.85E-03	51.8
EDAC	0.00198	4.4581	2.6421	1.55E-04	4.10E-04	54.8
CAN	0.00425	4.4377	2.7702	3.35E-04	9.28E-04	54.3
F.DOPA.GP.CS	0.00483	4.4666	3.0105	6.25E-04	1.88E-03	33.0

CONCLUSION

Conclusion

In this work, was synthesized MNPs of iron oxide by coprecipitation. The prepared nanoparticles have size of about 14 nm. The average size is in agreement with other literature. The result of structural characterization by diffraction of X-rays (the determination of the lattice parameter for Rietveld refinement) points to the formation of magnetite iron oxide crystallographic phase, although the presence of maghemite cannot be discharged.

The main objective of this study was to cover the iron oxide NPs with a biocompatible polymer, the chitosan through two different molecules (dopamine and caffeic acid) was achieved. The link between the iron oxide and the ligands agents was proved as well as the disaggregation of the iron oxide NPs. The tethering of the F.DOPA with genipin, was accomplished and proved. The shell of chitosan in the NPs are well observed in the NPs, proving that by these agents of functionalization and tethering, it is possible to coat the MNPs of iron oxide. All this results were confirmed by FTIR, TGA, TEM and DLS/Zeta Potential. The results of measurements of the hyperthermia show good and similar results between the different iron oxide coatings.

In future, the synthesis of iron oxide nanoparticles should be optimized in order to obtain more uniform size as well less aggregation, to be possible a more individualized coating.

The results in magnetization and hyperthermia are similar in the NPs. Test stability of the coated NPs should be one of the next steps.

BIBLIOGRAPHY

Bibliography

(1) World Health Organization http://www.who.int/mediacentre/factsheets/fs297/en/ (accessed Jan 26, 2016).

(2) World Cancer Report 2014 http://www.iarc.fr/en/publications/books/wcr/wcr-order.php (accessed Jan 26, 2016).

(3) Cancer Control: A Global Snaptshot in 2015 http://www.who.int/cancer/cancer-snapshot-2015/en/ (accessed Nov 4, 2016).

(4) Roy Chowdhury, M.; Schumann, C.; Bhakta-Guha, D.; Guha, G. Cancer Nanotheranostics: Strategies, Promises and Impediments. *Biomed. Pharmacother.* **2016**, *84*, 291–304.

(5) Périgo, E. A.; Hemery, G.; Sandre, O.; Ortega, D.; Garaio, E.; Plazaola, F.; Teran, F. J. Fundamentals and Advances in Magnetic Hyperthermia. *Appl. Phys. Rev.* **2015**, *2*, 41302.

(6) Ahmad, M. Z.; Alkahtani, S. A.; Akhter, S.; Ahmad, F. J.; Ahmad, J.; Akhtar, M. S.; Mohsin, N.; Abdel-Wahab, B. a. Progress in Nanotechnology-Based Drug Carrier in Designing of Curcumin Nanomedicines for Cancer Therapy: Current State-of-the-Art. *J. Drug Target.* **2015**, *24* (4), 273–293.

(7) Samadian, H.; Hosseini-Nami, S.; Kamrava, S. K.; Ghaznavi, H.; Shakeri-Zadeh, A. Folate-Conjugated Gold Nanoparticle as a New Nanoplatform for Targeted Cancer Therapy. *J. Cancer Res. Clin. Oncol.* **2016**, *142* (11), 1–13.

(8) Shevtsov, M. A.; Multhoff, G. Recent Developments of Magnetic Nanoparticles for Theranostics of Brain Tumor. *Curr. Drug Metab.* **2016**, 737–744.

(9) Karponis, D.; Azzawi, M.; Seifalian, A. An Arsenal of Magnetic Nanoparticles; Perspectives in the Treatment of Cancer. *Nanomedicine* **2016**, *11* (16), 2215–2232.

(10) Juang, S. H. R.; Huang, S.-H.; Juang, R.-S. Biochemical and Biomedical Applications of Multifunctional Magnetic Nanoparticles: A Review. *J. Nanoparticle Res.* **2011**, *13* (10), 4411–4430.

(11) Lodhia, J.; Mandarano, G.; Ferris, N. j.; Eu, P.; Cowell, S. F. Development and Use of Iron Oxide Nanoparticles (Part 1): Synthesis of Iron Oxide Nanoparticles for MRI.

Biomed. Imaging Interv. J. **2010**, *6* (2), 1–11.

(12) Jaiswal, M. K.; Gogoi, M.; Dev Sarma, H.; Banerjee, R.; Bahadur, D. Biocompatibility, Biodistribution and Efficacy of Magnetic Nanohydrogels in Inhibiting Growth of Tumors in Experimental Mice Models. *Biomater. Sci.* **2014**, *2*, 370.

(13) Laurent, S.; Mahmoudi, M. Superparamagnetic Iron Oxide Nanoparticles: Promises for Diagnosis and Treatment of Cancer. *Int. J. Mol. Epidemiol. Genet.* **2011**, *2* (4), 367–390.

(14) Mai, T. T. T.; Ha, P. T.; Pham, H. L. H. N.; Le, T. T. H.; Pham, H. L. H. N.; Phan, T. B. H.; Tran, D. L.; Nguyen, X. P. Chitosan and O-Carboxymethyl Chitosan Modified Fe3O4 for Hyperthermic Treatment. *Adv. Nat. Sci. Nanosci. Nanotechnol.* **2012**, *3* (1), 15006.

(15) Fan, C.; Gao, W.; Chen, Z. Z.; Fan, H.; Li, M.; Deng, F.; Chen, Z. Z. Tumor Selectivity of Stealth Multi-Functionalized Superparamagnetic Iron Oxide Nanoparticles. *Int. J. Pharm.* **2011**, *404* (1–2), 180–190.

(16) Lin, T.-C.; Lin, F.-H.; Lin, J.-C. In Vitro Characterization of Magnetic Electrospun IDA-Grafted Chitosan Nanofiber Composite for Hyperthermic Tumor Cell Treatment. *J. Biomater. Sci. Polym. Ed.* **2013**, *24* (9), 1152–1163.

(17) Shete, P. B.; Patil, R. M.; Tiwale, B. M.; Pawar, S. H. Water Dispersible Oleic Acid-Coated Fe3O4 Nanoparticles for Biomedical Applications. *J. Magn. Magn. Mater.* **2015**, *377*, 406–410.

(18) Patil, R. M.; Shete, P. B.; Thorat, N. D.; Otari, S. V.; Barick, K. C.; Prasad, A.; Ningthoujam, R. S.; Tiwale, B. M.; Pawar, S. H. Superparamagnetic Iron Oxide/chitosan Core/shells for Hyperthermia Application: Improved Colloidal Stability and Biocompatibility. *J. Magn. Magn. Mater.* **2014**, *355*, 22–30.

(19) Doyle, P. S.; Bibette, J.; Bancaud, A.; Viovy, J.-L. Self-Assembled Magnetic Matrices for DNA Separation Chips. *Science (80-.).* **2002**, *295* (5563), 2237 LP-2237.

(20) Wang, D.; He, J.; Rosenzweig, N.; Rosenzweig, Z. Superparamagnetic Fe2O3 Beads−CdSe/ZnS Quantum Dots Core−Shell Nanocomposite Particles for Cell Separation. *Nano Lett.* **2004**, *4* (3), 409–413.

(21) Gu, H.; Ho, P. L.; Tsang, K. W. T.; Wang, L.; Xu, B. Using Biofunctional Magnetic Nanoparticles to Capture Vancomycin-Resistant Enterococci and Other Gram-

Positive Bacteria at Ultralow Concentration. *J. Am. Chem. Soc.* **2003**, *125* (51), 15702–15703.

(22) Gupta, A. K.; Gupta, M. Synthesis and Surface Engineering of Iron Oxide Nanoparticles for Biomedical Applications. *Biomaterials* **2005**, *26* (18), 3995–4021.

(23) Jordan, A.; Scholz, R.; Wust, P.; Schirra, H.; Thomas Schiestel; Schmidt, H.; Felix, R. Endocytosis of Dextran and Silan-Coated Magnetite Nanoparticles and the Effect of Intracellular Hyperthermia on Human Mammary Carcinoma Cells in Vitro. *J. Magn. Magn. Mater.* **1999**, *194* (1), 185–196.

(24) Hilger, I.; Andrä, W.; Hergt, R.; Hiergeist, R.; Schubert, H.; Kaiser, W. A. Electromagnetic Heating of Breast Tumors in Interventional Radiology: In Vitro and in Vivo Studies in Human Cadavers and Mice. *Radiology* **2001**, *218* (13), 570–575.

(25) Hirsch, L. R.; Stafford, R. J.; Bankson, J. a; Sershen, S. R.; Rivera, B.; Price, R. E.; Hazle, J. D.; Halas, N. J.; West, J. L. Nanoshell-Mediated near-Infrared Thermal Therapy of Tumors under Magnetic Resonance Guidance. *Proc. Natl. Acad. Sci. U. S. A.* **2003**, *100* (23), 13549–13554.

(26) C.F. Chan, D.; B. Kirpotin, D.; A. Bunn, P. Synthesis and Evaluation of Colloidal Magnetic Iron Oxides for the Site-Specific Radiofrequency-Induced Hyperthermia of Cancer. *J. Magn. Magn. Mater.* **1993**, *122* (1), 374–378.

(27) Horsman, M. R.; Vaupel, P. Pathophysiological Basis for the Formation of the Tumor Microenvironment. *Front. Oncol.* **2016**, *6* (April), 66.

(28) Ahmad, R.; Ali, Z.; Mou, X.; Wang, J.; Yi, H.; He, N. Recent Advances in Magnetic Nanoparticle Design for Cancer Therapy. *J. Nanosci. Nanotechnol.* **2016**, *16* (9), 9393–9403.

(29) Kawashita, M.; Tanaka, M.; Kokubo, T.; Inoue, Y.; Yao, T.; Hamada, S.; Shinjo, T. Preparation of Ferrimagnetic Magnetite Microspheres for in Situ Hyperthermic Treatment of Cancer. *Biomaterials* **2005**, *26* (15), 2231–2238.

(30) Silva, F. A. S. da; Rojas, E. E. G.; Rodrigues, G. F.; Silva, B. F. A. da; Campos, M. F. de. SYNTHESIS AND CHARACTERIZATION OF BIOCOMPATIBLE Fe3O4 FOR USE IN CELL HYPERTHERMIA. *Mater. Sci. Forum* **2014**, *775–776*, 476–481.

(31) Maureen, L.; Awalpreet, S.; Kaur, P.; Aliru, M. L.; Chadha, A. S.; Asea, A.; Krishnan, S. Hyperthermia Using Nanoparticles - Promises and Pitfalls. *Int. J. Hyperth.* **2016**, *0*

(0), 1–13.

(32) Chen, B.; Wu, W.; Wang, X. Magnetic Iron Oxide Nnoparticles for Tumor-Targeted Therapy. *Curr. Cancer Drug Targets* **2011**, *11*, 184–189.

(33) Chen, Y.; Chen, B. A. Application and Development of Magnetic Iron- Oxide Nanoparticles in Tumor-Targeted Therapy (Review). *Chin. J. Cancer* **2010**, *29* (1), 118–122.

(34) Proença, M. J. P. de J. P. Magnetism at the Nanoscale: Nanoparticles, Nanowires, Nanotubes and Their Ordered Arrays, Universidade do Porto, 2012.

(35) Mahdavi, M.; Ahmad, M. Bin; Haron, J. M.; Namvar, F.; Nadi, B.; Rahman, M. Z. A.; Amin, J.; Haron, M. J.; Namvar, F.; Nadi, B.; Ab Rahman, M. Z.; Amin, J. Synthesis, Surface Modification and Characterisation of Biocompatible Magnetic Iron Oxide Nanoparticles for Biomedical Applications. *Molecules* **2013**, *18* (7), 7533–7548.

(36) Satalkar, P.; Elger, B. S.; Shaw, D. M. Defining Nano, Nanotechnology and Nanomedicine: Why Should It Matter? *Sci. Eng. Ethics* **2015**.

(37) What's So Special about the Nanoscale? https://www.nano.gov/nanotech-101/special (accessed Dec 11, 2016).

(38) William D. Callister, J. . D. G. R. *Materials Science and Engineering: An Introduction*, 8th ed.; 2010.

(39) Jacob, J. A.; Salmani, J. M. M.; Chen, B. Magnetic Nanoparticles: Mechanistic Studies on the Cancer Cell Interaction. *Nanotechnol. Rev.* **2016**, *5* (5), 481–488.

(40) Esmaeili, A.; Alizadeh Hadad, N. Preparation of ZnFe2O4–chitosan-Doxorubicin Hydrochloride Nanoparticles and Investigation of Their Hyperthermic Heat-Generating Characteristics. *Ceram. Int.* **2015**, *41* (6), 7529–7535.

(41) Santos, D. P.; Ruiz, M. A.; Gallardo, V.; Zanoni, M. V. B.; Arias, J. L. Multifunctional Antitumor Magnetite/Chitosan-L-Glutamic Acid (Core/Shell) Nanocomposites. *J. Nanoparticle Res.* **2011**, *13* (9), 4311–4323.

(42) Aadinath, W.; Ghosh, T.; Anandharamakrishnan, C. Multimodal Magnetic Nano-Carriers for Cancer Treatment: Challenges and Advancements. *J. Magn. Magn. Mater.* **2016**, *401*, 1159–1172.

(43) Zhang, F.; Xu, C.-L. L.; Liu, C.-M. M. Drug Delivery Strategies to Enhance the Permeability of the Blood–Brain Barrier for Treatment of Glioma. *Drug Des. Devel*

opment Ther. **2015**, *9*, 2089–2100.

(44) Qu, J.; Liu, G.; Wang, Y.; Hong, R. Preparation of Fe3O4–Chitosan Nanoparticles Used for Hyperthermia. *Adv. Powder Technol.* **2010**, *21* (4), 461–467.

(45) El-Hammadi, M. M.; Arias, J. L. Iron Oxide-Based Multifunctional Nanoparticulate Systems for Biomedical Applications: A Patent Review (2008 – Present). *Expert Opin. Ther. Pat.* **2015**, *25* (6), 691–709.

(46) Dabbagh, A.; Abdullah, B. J. J.; Abdullah, H.; Hamdi, M.; Kasim, N. H. A. Triggering Mechanisms of Thermosensitive Nanoparticles under Hyperthermia Condition. *J. Pharm. Sci.* **2015**, *104* (8), 2414–2428.

(47) Chiang, W.-H.; Huang, W.-C.; Chang, C.-W.; Shen, M.-Y.; Shih, Z.-F.; Huang, Y.-F.; Lin, S.-C.; Chiu, H.-C. Functionalized Polymersomes with Outlayered Polyelectrolyte Gels for Potential Tumor-Targeted Delivery of Multimodal Therapies and MR Imaging. *J. Control. Release* **2013**, *168* (3), 280–288.

(48) Donadel, K.; Felisberto, M. D. V.; Fávere, V. T.; Rigoni, M.; Batistela, N. J.; Laranjeira, M. C. M. Synthesis and Characterization of the Iron Oxide Magnetic Particles Coated with Chitosan Biopolymer. *Mater. Sci. Eng. C* **2008**, *28* (4), 509–514.

(49) Atsumi, T.; Jeyadevan, B.; Sato, Y.; Tohji, K. Heating Efficiency of Magnetite Particles Exposed to AC Magnetic Field. *J. Magn. Magn. Mater.* **2007**, *310* (2), 2841–2843.

(50) Vendrame, S. C. SÍNTESE, CARACTERIZAÇÃO E ANÁLISE DE CITOTOXICIDADE DE NANOPARTÍCULAS DE MAGNETITA PARA APLICAÇÕES BIOMÉDICAS, Unbiversidade Estadual do Centro-Oeste, 2011.

(51) Deatsch, A. E.; Evans, B. A. Heating Efficiency in Magnetic Nanoparticle Hyperthermia. *J. Magn. Magn. Mater.* **2014**, *354* (February), 163–172.

(52) Blanco-Andujar, C.; Walter, A.; Cotin, G.; Bordeianu, C.; Mertz, D.; Felder-Flesch, D.; Begin-Colin, S. Design of Iron Oxide-Based Nanoparticles for MRI and Magnetic Hyperthermia. *Nanomedicine* **2016**, *11* (14), 1889–1910.

(53) López-Quintela, M. A.; Piñeiro, Y.; Vargas, Z.; Rivas, J. Iron Oxide Based Nanoparticles for Magnetic Hyperthermia Strategies in Biological Applications. *Eur. J. Inorg. Chem.* **2015**, *2015* (27), 4495–4509.

(54) Lahiri, B. B.; Muthukumaran, T.; Philip, J. Magnetic Hyperthermia in Phosphate

Coated Iron Oxide Nanofluids. *J. Magn. Magn. Mater.* **2016**, *407*, 101–113.

(55) Zee, J. van der. Heating the Patient: A Promising Approach? (Review). *Ann. Oncol.* **2002**, *13* (8), 1173–1184.

(56) Besić, E. Physical Mechanisms and Methods Employed in Drug Delivery to Tumors. *Acta Pharm.* **2007**, *57* (3), 249–268.

(57) Patil, U. S.; Adireddy, S.; Jaiswal, A.; Mandava, S.; Lee, B. R.; Chrisey, D. B. In Vitro/In Vivo Toxicity Evaluation and Quantification of Iron Oxide Nanoparticles. *Int. J. Mol. Sci.* **2015**, *16* (10), 24417–24450.

(58) Pankhurst, Q. A.; Connolly, J.; Jones, S. K.; Dobson, J. Applications of Magnetic Nanoparticles in Biomedicine (TOPICAL REVIEW). *J. Phys. D. Appl. Phys.* **2003**, *36*, 167–181.

(59) Wang, H.; Shrestha, T. B.; Basel, M. T.; Pyle, M.; Toledo, Y.; Konecny, A.; Thapa, P.; Ikenberry, M.; Hohn, K. L.; Chikan, V.; Troyer, D. L.; Bossmann, S. H. Hexagonal Magnetite Nanoprisms: Preparation, Characterization and Cellular Uptake. *J. Mater. Chem. B* **2015**, *3* (23), 4647–4653.

(60) Yang, Q.; Lan, F.; Yi, Q.; Wu, Y.; Gu, Z. A Colloidal Assembly Approach to Synthesize Magnetic Porous Composite Nanoclusters for Efficient Protein Adsorption. *Nanoscale* **2015**, *7* (42), 17617–17622.

(61) Arteaga-cardona, F.; Rojas-rojas, K.; Costo, R.; Mendez-Rojas, M. A.; Rojas-Rrojas, K.; Costo, R.; Mendez-Rojas, M. A.; Hernando, A.; Presa, P. de la. Improving the Magnetic Heating by Disaggregating Nanoparticles. *J. Alloys Compd.* **2016**, *663*, 636–644.

(62) Sreeram, K. J.; Nidhin, M.; Nair, B. U. Synthesis of Aligned Hematite Nanoparticles on Chitosan–alginate Films. *Colloids Surfaces B Biointerfaces* **2009**, *71* (2), 260–267.

(63) Drummond, A. L. Desenvolvimento de Sistemas Magnéticos Nanoestruturados Para Aplicações Biomédicas, Universidade de Brasília, 2012.

(64) Roca, A. G.; Costo, R.; Rebolledo, A. F.; Veintemillas-Verdaguer, S.; Tartaj, P.; González-Carreño, T.; Morales, M. P.; Serna, C. J. Progress in the Preparation of Magnetic Nanoparticles for Applications in Biomedicine. *J. Phys. D. Appl. Phys.* **2009**, *42* (22), 224002–224012.

(65) Jayalekshmi, A. C.; Victor, S. P.; Sharma, C. P. Magnetic and Degradable Polymer/bioactive Glass Composite Nanoparticles for Biomedical Applications.

Colloids Surfaces B Biointerfaces **2013**, *101*, 196–204.

(66) Mou, X.; Ali, Z.; Li, S.; He, N. Applications of Magnetic Nanoparticles in Targeted Drug Delivery System. *J. Nanosci. Nanotechnol.* **2015**, *15* (1), 54–62.

(67) Kamali, S.; Pouryazdan, M.; Ghafari, M.; Itou, M.; Rahman, M.; Stroeve, P.; Hahn, H.; Sakurai, Y. Magnetization and Stability Study of a Cobalt-Ferrite-Based Ferrofluid. *J. Magn. Magn. Mater.* **2016**, *404*, 143–147.

(68) Park, E. J.; Kim, S. W.; Yoon, C.; Kim, Y.; Sung, J.; Kim, J. S. Disturbance of Ion Environment and Immune Regulation Following Biodistribution of Magnetic Iron Oxide Nanoparticles Injected Intravenously. *Toxicol. Lett.* **2016**, *243*, 67–77.

(69) Yang, L.; Kuang, H.; Zhang, W.; Aguilar, Z. P.; Xiong, Y.; Lai, W.; Xu, H.; Wei, H. Size Dependent Biodistribution and Toxicokinetics of Iron Oxide Magnetic Nanoparticles in Mice. *Nanoscale* **2015**, *7* (2), 625–636.

(70) Zarschler, K.; Rocks, L.; Licciardello, N.; Boselli, L.; Polo, E.; Garcia, K. P.; De Cola, L.; Stephan, H.; Dawson, K. A. Ultrasmall Inorganic Nanoparticles: State-of-the-Art and Perspectives for Biomedical Applications. *Nanomedicine Nanotechnology, Biol. Med.* **2016**, *12* (6), 1663–1701.

(71) Ruiz, A.; Gutiérrez, L.; Cáceres-Vélez, P. R.; Santos, D.; Chaves, S. B.; Fascineli, M. L.; Garcia, M. P.; Azevedo, R. B.; Morales, M. P. Biotransformation of Magnetic Nanoparticles as a Function of Coating in a Rat Model. *Nanoscale* **2015**, *7* (39), 16321–16329.

(72) van Landeghem, F. K. H.; Maier-Hauff, K.; Jordan, A.; Hoffmann, K. T.; Gneveckow, U.; Scholz, R.; Thiesen, B.; Brück, W.; von Deimling, A. Post-Mortem Studies in Glioblastoma Patients Treated with Thermotherapy Using Magnetic Nanoparticles. *Biomaterials* **2009**, *30* (1), 52–57.

(73) Shete, P. B. B.; Patil, R. M. M.; Thorat, N. D. D.; Prasad, A.; Ningthoujam, R. S. S.; Ghosh, S. J. J.; Pawar, S. H. H. Magnetic Chitosan Nanocomposite for Hyperthermia Therapy Application: Preparation, Characterization and in Vitro Experiments. *Appl. Surf. Sci.* **2014**, *288*, 149–157.

(74) Panta, P. C. Obtenção de Nanopertículas de Óxido de Ferro Por Coprecipitação, Sua Estabilização Com Surfactantes E Caracterização Quanto À Morfologia, Cristalinidade E Comportamento Magnético, Universidade Federal do Rio Grande do Sul, 2013.

(75) Dorniani, D.; Hussein, M. Z. Bin; Kura, A. U.; Fakurazi, S.; Shaari, A. H.; Ahmad, Z. Preparation of Fe3O4 Magnetic Nanoparticles Coated with Gallic Acid for Grug Delivery. *Int. J. Nanomedicine* **2012**, *7*, 5745–5756.

(76) Cunha, S.; Superior, E. Aplicação de Nanopartículas Magnéticas Em Hipertermia Novembro 2014. **2014**.

(77) Choi, H. S.; Liu, W.; Misra, P.; Tanaka, E.; Zimmer, J. P.; Itty Ipe, B.; Bawendi, M. G.; Frangioni, J. V. Renal Clearance of Quantum Dots. *Nat. Biotechnol.* **2007**, *25* (10), 1165–1170.

(78) Xu, H.; Cui, L.; Tong, N.; Gu, H. Development of High Magnetization Fe3O4/polystyrene/ Silica Nanospheres via Combined Miniemulsion/emulsion Polymerization. *J. Am. Chem. Soc.* **2006**, *128* (49), 15582–15583.

(79) Jadhav, N. V.; Prasad, A. I.; Kumar, A.; Mishra, R.; Dhara, S.; Babu, K. R.; Prajapat, C. L.; Misra, N. L.; Ningthoujam, R. S.; Pandey, B. N.; Vatsa, R. K. Synthesis of Oleic Acid Functionalized Fe3O4 Magnetic Nanoparticles and Studying Their Interaction with Tumor Cells for Potential Hyperthermia Applications. *Colloids Surfaces B Biointerfaces* **2013**, *108*, 158–168.

(80) Menelaou, M.; Georgoula, K.; Simeonidis, K.; Dendrinou-Samara, C. Evaluation of Nickel Ferrite Nanoparticles Coated with Oleylamine by NMR Relaxation Measurements and Magnetic Hyperthermia. *Dalton Trans.* **2014**, *43* (9), 3626–3636.

(81) Xu, C.; Xu, K.; Gu, H.; Zheng, R.; Liu, H.; Zhang, X.; Guo, Z.; Xu, B. Dopamine as A Robust Anchor to Immobilize Functional Molecules on the Iron Oxide Shell of Magnetic Nanoparticles. *J. Am. Chem. Soc.* **2004**, *126* (32), 9938–9939.

(82) Ali, A.; Zafar, H.; Zia, M.; Ul Haq, I.; Phull, A. R.; Ali, J. S.; Hussain, A. Synthesis, Characterization, Applications, and Challenges of Iron Oxide Nanoparticles. *Nanotechnol. Sci. Appl.* **2016**, *9*, 49–67.

(83) Zhang, W.; Jia, S. Y.; Wu, S. H.; Zhang, S. F.; Liu, Y. Effects of Alkaline Precipitating Agents on Synthesis of Magnetite Nanomaterials by Hydrothermal D-Glucose Method. *J. Nanoparticle Res.* **2013**, *15* (6).

(84) Baykal, A.; Amir, M.; Günerb, S.; Sözeri, H. Preparation and Characterization of SPION Functionalized via Caffeic Acid. *J. Magn. Magn. Mater.* **2015**, *395*, 199–204.

(85) Lee, S. J.; Choi, K.-C.; Kang, M.-S.; Oh, J.-S.; Jeong, Y.-I.; Lee, H. C. Self-Organized Nanoparticles of Caffeic Acid Conjugated Polysaccharide and Its Anticancer

Activity. *J. Nanosci. Nanotechnol.* **2015**, *15* (2), 1130–1134.

(86) Song, X.; Gu, X.; Sun, H.; Fu, C.; Zhang, Y.; Dong, P. Biomimetic Modification and In Vivo Safety Assessment of Superparamagnetic Iron Oxide Nanoparticles. *J. Nanosci. Nanotechnol.* **2016**, *16* (4), 4100–4107.

(87) Babic, M.; Horak, D.; Jendelova, P.; Herynek, V.; Proks, V.; Vanecek, V.; Lesny, P.; Sykova, E. The Use of Dopamine-Hyaluronate Associatecoated Maghemite Nanoparticles to Label Cells. *Int. J. Nanomedicine* **2012**, *7*, 1461–1474.

(88) Wang, L.; Yan, Y.; Wang, M.; Yang, H.; Zhou, Z.; Peng, C.; Yang, S. An Integrated Nanoplatform for Theranostics via Multifunctional Core-Shell Ferrite Nanocubes. *J. Mater. Chem. B* **2016**, *4* (10), 1908–1914.

(89) Wei, H.; Insin, N.; Lee, J.; Han, H. S.; Cordero, J. M.; Liu, W.; Bawendi, M. G. Compact Zwitterion-Coated Iron Oxide Nanoparticles for Biological Applications. *Nano Lett.* **2012**, *12* (1), 22–25.

(90) Ma, X.; Gong, A.; Chen, B.; Zheng, J.; Chen, T.; Shen, Z.; Wu, A. Exploring a New SPION-Based MRI Contrast Agent with Excellent Water-Dispersibility, High Specificity to Cancer Cells and Strong MR Imaging Efficacy. *Colloids Surfaces B Biointerfaces* **2015**, *126*, 44–49.

(91) Shah, S. A.; Majeed, A.; Rashid, K.; Awan, S. U. PEG-Coated Folic Acid-Modified Superparamagnetic MnFe2O 4 Nanoparticles for Hyperthermia Therapy and Drug Delivery. *Mater. Chem. Phys.* **2013**, *138* (2–3), 703–708.

(92) Muñoz-Bonilla, A.; Marcelo, G.; Casado, C.; Teran, F. J.; Fernández-García, M. Preparation of Glycopolymer-Coated Magnetite Nanoparticles for Hyperthermia Treatment. *J. Polym. Sci. Part A Polym. Chem.* **2012**, *50* (24), 5087–5096.

(93) Blanco-Andujar, C.; Ortega, D.; Southern, P.; Pankhurst, Q. a; Thanh, N. T. K. High Performance Multi-Core Iron Oxide Nanoparticles for Magnetic Hyperthermia: Microwave Synthesis, and the Role of Core-to-Core Interactions. *Nanoscale* **2015**, *7* (5), 1768–1775.

(94) de Sousa, M. E.; Fernández van Raap, M. B.; Rivas, P. C.; Mendoza Zélis, P.; Girardin, P.; Pasquevich, G. A.; Alessandrini, J. L.; Muraca, D.; Sánchez, F. H. Stability and Relaxation Mechanisms of Citric Acid Coated Magnetite Nanoparticles for Magnetic Hyperthermia. *J. Phys. Chem. C* **2013**, *117* (10), 5436–5445.

(95) Barick, K. C.; Singh, S.; Bahadur, D.; Lawande, M. A.; Patkar, D. P.; Hassan, P. A.

Carboxyl Decorated Fe3O4 Nanoparticles for MRI Diagnosis and Localized Hyperthermia. *J. Colloid Interface Sci.* **2014**, *418*, 120–125.

(96) Kim, D. H.; Kim, K. N.; Kim, K. M.; Lee, Y. K. Targeting to Carcinoma Cells with Chitosan- and Starch-Coated Magnetic Nanoparticles for Magnetic Hyperthermia. *J. Biomed. Mater. Res. - Part A* **2009**, *88* (1), 1–11.

(97) Arias, J. L.; Reddy, L. H.; Couvreur, P. Fe3O4/chitosan Nanocomposite for Magnetic Drug Targeting to Cancer. *J. Mater. Chem.* **2012**, *22*, 7622.

(98) Saravanakumar, T.; Palvannan, T.; Kim, D. H.; Park, S. M. Optimized Immobilization of Peracetic Acid Producing Recombinant Acetyl Xylan Esterase on Chitosan Coated-Fe3O4 Magnetic Nanoparticles. *Process Biochem.* **2014**, *49* (11), 1920–1928.

(99) Xiao, W.; Liu, X.; Hong, X.; Yang, Y.; Lv, Y.; Fang, J.; Ding, J. Magnetic-Field-Assisted Synthesis of Magnetite Nanoparticles via Thermal Decomposition and Their Hyperthermia Properties. *CrystEngComm* **2015**, *17* (19), 3652–3658.

(100) Soares, P. I. P.; Machado, D.; Laia, C.; Pereira, L. C. J.; Coutinho, J. T.; Ferreira, I. M. M.; Novo, C. M. M.; Borges, J. P. Thermal and Magnetic Properties of Chitosan-Iron Oxide Nanoparticles. *Carbohydr. Polym.* **2016**, *149*, 382–390.

(101) Liu, J.; Wen, X. yuan; Lu, J. feng; Kan, J.; Jin, C. hai. Free Radical Mediated Grafting of Chitosan with Caffeic and Ferulic Acids: Structures and Antioxidant Activity. *Int. J. Biol. Macromol.* **2014**, *65*, 97–106.

(102) Tsai, Y.-L. T. H.-C. L. P.-I. C. C.-J. L. H.-T. L. Y.-C. Synthesis and Characterization of Superparamagnetic Fe3O4-SiO2 Nanoparticles. *Int. J. Nanotechnol.* **2013**, *10* (10), 916–929.

(103) Silva, V. A. J.; Andrade, P. L.; Silva, M. P. C.; Bustamante, A. D.; De Los Santos Valladares, L.; Albino Aguiar, J. Synthesis and Characterization of Fe3O4 Nanoparticles Coated with Fucan Polysaccharides. *J. Magn. Magn. Mater.* **2013**, *343*, 138–143.

(104) Kondaveeti, S.; Cornejo, D. R.; Petri, D. F. S. Alginate/magnetite Hybrid Beads for Magnetically Stimulated Release of Dopamine. *Colloids Surfaces B Biointerfaces* **2016**, *138*, 94–101.

(105) Gupta, A. K.; Gupta, M. Cytotoxicity Suppression and Cellular Uptake Enhancement of Surface Modified Magnetic Nanoparticles. *Biomaterials* **2005**, *26* (13), 1565–1573.

(106) Durdureanu-Angheluta, A.; Dascalu, A.; Fifere, A.; Coroaba, A.; Pricop, L.; Chiriac, H.; Tura, V.; Pinteala, M.; Simionescu, B. C. Progress in the Synthesis and Characterization of Magnetite Nanoparticles with Amino Groups on the Surface. *J. Magn. Magn. Mater.* **2012**, *324* (9), 1679–1689.

(107) Bootdee, K.; Nithitanakul, M.; Grady, B. P. Synthesis and Encapsulation of Magnetite Nanoparticles in PLGA: Effect of Amount of PLGA on Characteristics of Encapsulated Nanoparticles. *Polym. Bull.* **2012**, *69* (7), 795–806.

(108) Morales, M. A.; Jain, T. K.; Labhasetwar, V.; Leslie-Pelecky, D. L. Magnetic Studies of Iron Oxide Nanoparticles Coated with Oleic Acid and Pluronic?? Block Copolymer. *J. Appl. Phys.* **2005**, *97* (10), 2005–2008.

(109) Liu, X. L.; Fan, H. M.; Yi, J. B.; Yang, Y.; Choo, E. S. G.; Xue, J. M.; Fan, D. Di; Ding, J. Optimization of Surface Coating on Fe3O4 Nanoparticles for High Performance Magnetic Hyperthermia Agents. *J. Mater. Chem.* **2012**, *22* (17), 8235.

(110) Nguyen, D. H.; Lee, J. S.; Choi, J. H.; Park, K. M.; Lee, Y.; Park, K. D. Hierarchical Self-Assembly of Magnetic Nanoclusters for Theranostics: Tunable Size, Enhanced Magnetic Resonance Imagability, and Controlled and Targeted Drug Delivery. *Acta Biomater.* **2016**, *35*, 109–117.

(111) Kolosnjaj-Tabi, J.; Di Corato, R.; Lartigue, L.; Marangon, I.; Guardia, P.; Silva, A. K. A.; Luciani, N.; Clément, O.; Flaud, P.; Singh, J. V.; Decuzzi, P.; Pellegrino, T.; Wilhelm, C.; Gazeau, F. Heat-Generating Iron Oxide Nanocubes: Subtle "destructurators" of the Tumoral Microenvironment. *ACS Nano* **2014**, *8* (5), 4268–4283.

(112) Abdulla-Al-Mamun, M.; Kusumoto, Y.; Zannat, T.; Horie, Y.; Manaka, H. Au-Ultrathin Functionalized Core–shell (Fe3O4@Au) Monodispersed Nanocubes for a Combination of Magnetic/plasmonic Photothermal Cancer Cell Killing. *RSC Adv.* **2013**, *3* (21), 7816.

(113) Knežević, N. Ž.; Ruiz-Hernández, E.; Hennink, W. E.; Vallet-Regí, M. Magnetic Mesoporous Silica-Based Core/shell Nanoparticles for Biomedical Applications. *RSC Adv.* **2013**, *3* (25), 9584.

(114) Arcos, D.; Fal-Miyar, V.; Ruiz-Hernández, E.; Garcia-Hernández, M.; Ruiz-González, M. L.; González-Calbet, J.; Vallet-Regí, M. Supramolecular Mechanisms in the Synthesis of Mesoporous Magnetic Nanospheres for Hyperthermia. *J. Mater.*

Chem. **2012**, *22* (1), 64.

(115) Souza, K. C.; Mohallem, N. D. S.; Sousa, E. M. B. Mesoporous Silica-Magnetite Nanocomposite: Facile Synthesis Route for Application in Hyperthermia. *J. Sol-Gel Sci. Technol.* **2010**, *53* (2), 418–427.

(116) Bini, R. A.; Marques, R. F. C.; Santos, F. J.; Chaker, J. A.; Jafelicci, M. Synthesis and Functionalization of Magnetite Nanoparticles with Different Amino-Functional Alkoxysilanes. *J. Magn. Magn. Mater.* **2012**, *324* (4), 534–539.

(117) Tumturk, H.; Sahin, F.; Turan, E. Magnetic Nanoparticles Coated with Different Shells for Biorecognition: High Specific Binding Capacity. *Analyst* **2014**, *139* (5), 1093–1100.

(118) KIM, C.-Y.; XU, L.; Mao, Q.; LEE, E.-H. Magnetic Silicone Composites with Uniform Nanoparticle Dispersion as a Biomedical Stent Coating for Hyperthermia. *Adv. Polym. Technol.* **2012**, *32* (2013), 474–485.

(119) Harraz, F. a. Synthesis and Surface Properties of Magnetite (Fe3O4) Nanoparticles Infiltrated into Porous Silicon Template. *Appl. Surf. Sci.* **2013**, *287* (May), 203–210.

(120) Tavaria, F. K.; Costa, E. M.; Pina-Vaz, I.; Carvalho, M. F.; Pintado, M. M. A Quitosana Como Biomaterial Odontológico: Estado Da Arte. *Rev. Bras. Eng. Biomed.* **2013**, *29* (1), 110–120.

(121) Chang, K. P.; Cheng, C. H.; Chiang, Y. C.; Lee, S. C.; Lin, C. Y.; Hsieh, B. T.; Ko, C. C.; Huang, Y. L. Irradiation of Synthesized Magnetic Nanoparticles and Its Application for Hyperthermia. *Adv. Mater. Res.* **2008**, *47–50*, 1298–1301.

(122) Bae, K. H.; Park, M.; Do, M. J.; Lee, N.; Ryu, J. H.; Kim, G. W.; Kim, C.; Park, T. G.; Hyeon, T. Chitosan Oligosaccharide-Stabilized Ferrimagnetic Iron Oxide Nanocubes for Magnetically Modulated Cancer Hyperthermia. *ACS Nano* **2012**, *6* (6), 5266–5273.

(123) Thorat, N. D.; Bohara, R. A.; Malgras, V.; Tofail, S. A. M.; Ahamad, T.; Alshehri, S. M.; Wu, K. C.-W.; Yamauchi, Y. Multimodal Superparamagnetic Nanoparticles with Unusually Enhanced Specific Absorption Rate for Synergetic Cancer Therapeutics and Magnetic Resonance Imaging. *ACS Appl. Mater. Interfaces* **2016**, acsami.6b02616.

(124) Pereira, P. A. C. Nanogéis de Glicol Quitosano, Universidade do Minho, 2014.

(125) Ruini, F.; Tonda-Turo, C.; Chiono, V.; Ciardelli, G. Chitosan Membranes for Tissue

Engineering: Comparison of Different Crosslinkers. *Biomed. Mater.* **2015**, *10* (6), 65002.

(126) Nunes, C.; Maricato, É.; Cunha, Â.; Nunes, A.; Silva, J. a L. Da; Coimbra, M. a. Chitosan-Caffeic Acid-Genipin Films Presenting Enhanced Antioxidant Activity and Stability in Acidic Media. *Carbohydr. Polym.* **2013**, *91* (1), 236–243.

(127) Laurent, S.; Dutz, S.; Häfeli, U. O.; Mahmoudi, M. Magnetic Fluid Hyperthermia: Focus on Superparamagnetic Iron Oxide Nanoparticles. *Adv. Colloid Interface Sci.* **2011**, *166* (1–2), 8–23.

(128) Ingham, B. X-Ray Scattering Characterisation of Nanoparticles. *Crystallogr. Rev.* **2015**, *21* (4), 1–75.

(129) Hammonf, C. *The Basics of Crystallography and Difrractions*; Oxford University Press, 2009.

(130) Naiim, M.; Boualem, A.; Ferre, C.; Jabloun, M.; Jalocha, A.; Ravier, P. Multiangle Dynamic Light Scattering for the Improvement of Multimodal Particle Size Distribution Measurements. *Soft Matter* **2015**, *11* (28), 28–32.

(131) Podaru, G.; Moore, J.; Dani, R. K.; Prakash, P.; Chikan, V. Nested Helmholtz Coil Design for Producing Homogeneous Transient Rotating Magnetic Fields. *Rev. Sci. Instrum.* **2015**, *86* (3).

(132) Yazdani, F.; Seddigh, M. Magnetite Nanoparticles Synthesized by Co-Precipitation Method : The Effects of Various Iron Anions on Speci Fi Cations. *Mater. Chem. Phys.* **2016**, *184*, 2–7.

(133) Paul, G.; Kumar Das, P.; Manna, I. Synthesis, Characterization and Studies on Magneto-Viscous Properties of Magnetite Dispersed Water Based Nanofluids. *J. Magn. Magn. Mater.* **2016**, *404*, 29–39.

(134) Meng, Q.; Liu, J.; Zhang, C.; Wang, Z.; Liu, J.; Wang, Z. Chemical Synthesis and Characterization of Magnetic Nanoparticles, 2015, 1–6.

(135) Faraji, M.; Yamini, Y.; Rezaee, M. Magnetic Nanoparticles: Synthesis, Stabilization, Functionalization, Characterization, and Applications. *J. Iran. Chem. Soc.* **2010**, *7* (1), 1–37.

(136) Rochelle M. Cornell, U. S. *The Iron Oxides: Structure, Properties, Reactions, Occurrences and Uses*, 2 nd.; 2006.

(137) Vereda, F.; Rodríguez-González, B.; de Vicente, J.; Hidalgo-Álvarez, R. Evidence of

Direct Crystal Growth and Presence of Hollow Microspheres in Magnetite Particles Prepared by Oxidation of Fe(OH)2. *J. Colloid Interface Sci.* **2008**, *318* (2), 520–524.

(138) Stoia, M.; Istratie, R.; Păcurariu, C. Investigation of Magnetite Nanoparticles Stability in Air by Thermal Analysis and FTIR Spectroscopy. *J. Therm. Anal. Calorim.* **2016**, *125* (3), 1185–1198.

(139) Mahmoudi, M.; Sant, S.; Wang, B.; Laurent, S.; Sen, T. Superparamagnetic Iron Oxide Nanoparticles (SPIONs): Development, Surface Modification and Applications in Chemotherapy. *Adv. Drug Deliv. Rev.* **2011**, *63* (1–2), 24–46.

(140) Abràmoff, M. D.; Magalhães, P. J.; Ram, S. J. Image Processing with ImageJ Second Edition. *Biophotonics Int.* **2004**, *11* (7), 36–42.

(141) Goya, G. F.; Berquó, T. S.; Fonseca, F. C.; Morales, M. P. Static and Dynamic Magnetic Properties of Spherical Magnetite Nanoparticles. *J. Appl. Phys.* **2003**, *94* (5), 3520–3528.

(142) Durgadas, C. V.; Sharma, C. P.; Sreenivasan, K. Fluorescent and Superparamagnetic Hybrid Quantum Clusters for Magnetic Separation and Imaging of Cancer Cells from Blood. *Nanoscale* **2011**, *3* (11), 4780–4787.

(143) Li, Y.; Zhu, H.; Hou, C.; Li, Y.; Zhao, G.; Liu, X.; Hou, K. One-Pot Solvothermal Synthesis of Highly Water-Dispersible Size-Tunable Functionalized Magnetite Nanocrystal Clusters for Lipase Immobilization. *Chem. - An Asian J.* **2013**, *8* (7), 1447–1454.

(144) Gunasekaran, S.; Thilak Kumar, R.; Ponnusamy, S. Vibrational Spectra and Normal Coordinate Analysis of Adrenaline and Dopamine. *Indian J. Pure Appl. Phys.* **2007**, *45* (11), 884–892.

(145) Long, Y.; Liang, K.; Niu, J.; Tong, X.; Yuan, B.; Ma, J. Agglomeration of Pd^{0} Nanoparticles Causing Different Catalytic Activities of Suzuki Carbonylative Cross-Coupling Reactions Catalyzed by Pd^{II} and Pd^{0} Immobilized on Dopamine-Functionalized Magnetite Nanoparticles. *New J. Chem.* **2015**, *39* (4), 2988–2996.

(146) Butler, M. F.; Ng, Y. F.; Pudney, P. D. A. Mechanism and Kinetics of the Crosslinking Reaction between Biopolymers Containing Primary Amine Groups and Genipin. *J. Polym. Sci. Part A Polym. Chem.* **2003**, *41* (24), 3941–3953.

(147) Klein, M. P.; Hackenhaar, C. R.; Lorenzoni, A. S. G.; Rodrigues, R. C.; Costa, T. M. H.; Ninow, J. L.; Hertz, P. F. Chitosan Crosslinked with Genipin as Support Matrix

for Application in Food Process: Support Characterization and β-D-Galactosidase Immobilization. *Carbohydr. Polym.* **2016**, *137*, 184–190.

(148) Delmar, K.; Bianco-Peled, H. The Dramatic Effect of Small pH Changes on the Properties of Chitosan Hydrogels Crosslinked with Genipin. *Carbohydr. Polym.* **2015**, *127*, 28–37.

(149) Zu, Y.; Yu, X.; Zhao, X.; Wang, W.; Wang, K. Nanocrystallization of the Pharmaceutically Active Agent Genipin by an Emulsion Solvent Evaporation Method. *J. Nanomater.* **2014**, *2014*.

(150) Hisham, S. F.; Kasim, S. H.; Abu Bakar, S.; Mohd Sabri, S. N.; Mastor, A.; Abdul Manaf, A. Y.; Abu, N.; Noorsal, K.; Abdul Rashid, A. H. Cross-Linked Effects by Genipin on Physicochemical Properties of Chitosan Film. *Adv. Mater. Res.* **2016**, *1133*, 108–112.

(151) Mi, F. L.; Shyu, S. S.; Peng, C. K. Characterization of Ring-Opening Polymerization of Genipin and pH-Dependent Cross-Linking Reactions between Chitosan and Genipin. *J. Polym. Sci. Part A Polym. Chem.* **2005**, *43* (10), 1985–2000.

(152) Madhavan, K.; Belchenko, D.; Tan, W. Roles of Genipin Crosslinking and Biomolecule Conditioning in Collagen-Based Biopolymer: Potential for Vascular Media Regeneration. *J. Biomed. Mater. Res. - Part A* **2011**, *97 A* (1), 16–26.

(153) Baykal, A.; Erdemi, H.; Amir, M. Temperature and Frequency Dependence on Electrical Properties of Fe3O4@ Caffeic Acid Nanocomposite. *J. Inorg. Organomet. Polym. Mater.* **2016**, *26* (1), 190–196.

(154) Świsłocka, R. Spectroscopic (FT-IR, FT-Raman, UV Absorption, 1H and 13C NMR) and Theoretical (in B3LYP/6-311++G** Level) Studies on Alkali Metal Salts of Caffeic Acid. *Spectrochim. Acta - Part A Mol. Biomol. Spectrosc.* **2013**, *100*, 21–30.

(155) Guo, D.; Dou, D.; Ge, L.; Huang, Z.; Wang, L.; Gu, N. A Caffeic Acid Mediated Facile Synthesis of Silver Nanoparticles with Powerful Anti-Cancer Activity. *Colloids Surfaces B Biointerfaces* **2015**, *134*, 229–234.

(156) Soliman, G. M.; Zhang, Y. L.; Merle, G.; Cerruti, M.; Barralet, J. Hydrocaffeic Acid-Chitosan Nanoparticles with Enhanced Stability, Mucoadhesion and Permeation Properties. *Eur. J. Pharm. Biopharm.* **2014**, *88* (3), 1026–1037.

(157) Anjaneyulu, U.; Swaroop, V. K.; Vijayalakshmi, U. Preparation and Characterization of Novel Ag Doped hydroxyapatite–Fe_3O_4–chitosan Hybrid Composites and in

Vitro Biological Evaluations for Orthopaedic Applications. *RSC Adv.* **2016**, *6* (13), 10997–11007.

(158) Nancy L. Delgadillo-Armendariza, Norma A. Rangel-Vazqueza,*, Edgar A. Marquez-Brazonb, c and B. R.-D. G. INTERACTIONS OF CHITOSAN/GENIPIN HYDROGELS DURING DRUG DELIVERY: A QSPR APPROACH. *Quim. Nov.* **2014**, *37* (9), 1503–1509.

(159) Polydispersity – what does it mean for DLS and chromatography? http://www.materials-talks.com/blog/2014/10/23/polydispersity-what-does-it-mean-for-dls-and-chromatography/ (accessed Dec 14, 2016).

ANNEX

Table S1-Additional information about the used reagents.

Reagent	Chemical formula	Purity	Brand
2-(N-Morpholino)ethanesulfonic acid hydrate (MES hydrated)	$C_6H_{13}NO_4S \cdot xH_2O$	99,5%	Sigma-Aldrich
acetic acid	CH_3COOH	≥99,7%	
ammonium hydroxide	NH_4OH	28-30%	
caffeic acid	$C_9H_8O_4$	≥98%	
chitosan (medium molecular weight) deacetylation degree=75-85%	$(C_6H_{11}NO_4)_n$	--	
dopamine hydrochloride	$(HO)_2C_6H_3CH_2CH_2NH_2 \cdot HCl$	98%	
iron (II) chloride tetrahydrate	$FeCl_2 \cdot 4H_2O$	≥99.0%	
Iron (III) chloride	$FeCl_3$	97%	
Isopropyl alcohol	C_3H_8O	≥99,8%	
1-Ethyl-3-(3-dimethylaminopropyl) carbodiimide (EDC)	$C_8H_{17}N_3 \cdot HCl$	≥99,5%	
ethanol	C_2H_6O	>99,8%	Carlos Erba
genipin	$C_{11}H_{14}O_5$	98%	Challenge Bioproducts Co
***N*-Hydroxysuccinimide**	$C_4H_5NO_3$	>98%	TCI